POLITECNICO DI TORINO
Repository ISTITUZIONALE

Free vibration analysis of sandwich plates by component-wise approach

Original
Free vibration analysis of sandwich plates by component-wise approach / Carrera, E., Abu Salem, K., Augello, R.. - In: THIN-WALLED STRUCTURES. - ISSN 0263-8231. - 218:(2026). [10.1016/j.tws.2025.114062]

Availability:
This version is available at: 11583/3017455 since: 2026-11-03T10:49:15Z

Publisher:
Elsevier

Published
DOI:10.1016/j.tws.2025.114062

Terms of use:

This article is made available under terms and conditions as specified in the corresponding bibliographic description in the repository

Publisher copyright

(Article begins on next page)

07 November 2026

Thin–Walled Structures 218 (2026) 114062

Contents lists available at ScienceDirect

Thin-Walled Structures

journal homepage: www.elsevier.com/locate/tws

Free vibration analysis of sandwich plates by component-wise approach

E. Carrera, K. Abu Salem *, R. Augello

Department of Mechanical and Aerospace Engineering, Politecnico di Torino, Corso Duca degli Abruzzi 24, 10129 Torino, Italy

ARTICLE INFO

Keywords:
CUF
FEM
Sandwich
Modal analysis
Structural modelling

ABSTRACT

This paper presents a comparative analysis of the linear response of sandwich structures with honeycomb cores, evaluated through different theoretical formulations implemented employing the Carrera Unified Formulation (CUF). This framework makes it possible to generate models with different levels of refinement, ranging from simplified to fully detailed descriptions. If the total structure is considered as a single layer, the Equivalent-Single Layer (ESL) is employed; if the skins and core are considered as components, the Layer-Wise (LW) is used; finally, the actual geometry of the core can be considered, along with the skin, leading to the Component-Wise (CW) approach. The research aims to assess the impact of the simplifications inherent in the ESL and LW models on the accuracy of modal predictions relative to the more detailed CW approach. A benchmark case is analysed, and its natural frequencies and mode shapes are computed using all three approaches and compared with results obtained from commercial two- and tree-dimensional finite elements. The outcomes reveal that although the ESL and LW models are computationally efficient and can capture the global deformation of the structure, they fail to address local effects, which are accurately predicted by the CW model. The latter, hence, is necessary to provide precise information about the dynamic behaviour of the honeycomb sandwich structure. In particular, Modal Assurance Criterion (MAC) values between the modes of the skins assessed by means of LW and CW, show that even if a global mode shape can be well represented by LW, local effects can only be detected by CW approach. This difference introduce an underestimation in the evaluated frequencies, which achieves -19 % and -10 % in case of bending and torsional modes within the first ten modes, respectively. Given the widespread use of honeycomb sandwich panels in aerospace structures for their high stiffness-to-weight ratio and vibro-acoustic insulation properties, the results underline the importance of adopting refined CW-based CUF models whenever accurate predictions of the dynamic response are required.

1. Introduction

Sandwich structures with honeycomb cores represent a class of advanced materials that have attracted considerable attention over recent decades due to their peculiar combination of low weight and high stiffness [1–4]. These structures, composed of two thin and rigid face sheets separated by an internal core characterized by a honeycomb architecture, offer an excellent strength-to-weight ratio; such attributes make them particularly suitable for applications in aerospace, automotive, and in general in high performance industrial environment [5–7]. The increasing demand for lighter and more efficient structures has driven intense interest in the numerical modelling of the mechanical response of these sandwich panels, particularly with regard to their modal and dynamic behaviour. Indeed, vibrational response of such structures is relevant to different engineering problems [8–15].

The geometric complexity of the honeycomb core and the occurrence of multiple scales of deformation make it challenging to develop accurate dynamic models with a reasonable computational cost, thereby posing a significant challenge in the design and optimization of structural systems. The literature presents several theories aimed at addressing the complexity inherent in modelling these structures. Homogenization-based approaches, such as the Equivalent Single Layer (ESL) and Layer-Wise (LW) theories, seek to replace the intricate hexagonal lattice with an equivalent material endowed with averaged mechanical properties [16–18]. These methods simplify the description of the overall structural behaviour and considerably reduce the number of degrees of freedom required for the analysis. In particular, the ESL theory considers the entire sandwich panel as a single homogeneous layer [19]; concurrently, the LW theory introduces a more refined discretization along the thickness direction by assigning independent variables to each layer of the structure, enhancing the representation of local deformations [20]. A LW formulation including third-order

* Corresponding author.
E-mail addresses: erasmo.carrera@polito.it (E. Carrera), karim.abusalem@polito.it (K. Abu Salem), riccardo.augello@polito.it (R. Augello).

https://doi.org/10.1016/j.tws.2025.114062
Received 8 July 2025; Received in revised form 16 September 2025; Accepted 5 October 2025
Available online 7 October 2025
0263-8231/© 2025 The Author(s). Published by Elsevier Ltd. This is an open access article under the CC BY license (http://creativecommons.org/licenses/by/4.0/).

thickness and shear deformation has been proposed for nonlinear analysis of sandwich panels in ref., [21], discussing the versatility of LW kinematic models. Advanced models have been developed for laminated shells using higher-order theories, offering enhanced accuracy in nonlinear regimes, see ref., [22].

Although both homogenization-based models offer advantages in terms of computational efficiency and ease of implementation, they exhibit limitations in capturing the local interactions between the core and the skins. For the aforementioned reasons, a more accurate representation of the structure is required. The only viable approach is the Finite Element Method (FEM) using commercial software, necessitating a fully three-dimensional modelling strategy. A reliable 3D FEM model capable of capturing through-thickness response with sufficient accuracy requires at least three to four solid elements across the thickness of the structure. However, the core and skins of sandwich structures are inherently extremely thin components, leading to a substantially large number of degrees of freedom. In light of these limitations, the need has emerged to adopt higher-fidelity modelling approaches, such as the Component-Wise (CW) methodology. Contrary to the homogenized approaches, the CW approach models each component of the structure, i.e. honeycomb core and top/bottom skins, as an independent subdomain, thus avoiding simplifications that might neglect relevant local effects. This allows for the actual representation of different possible core geometries, as those described in ref., [23,24]. Another substructuring technique worth mentioning is the artificial spring method, see ref., [25], which introduces distributed elastic constraints at interfaces to model coupling between structural components. Unlike the CW approach, which enforces exact continuity through shared displacement fields, the artificial spring method relies on assumed stiffness parameters to approximate interface behaviour. The CW modelling approach reproduces the actual geometry and allows for a detailed analysis of the interactions between the different parts, providing a more accurate representation of the structure mechanical behaviour. Despite its higher fidelity, especially for the resolution of local phenomena, the CW model requires a higher computational load and greater implementation complexity, factors that often limit its application in engineering contexts where the trade-off between precision and computational cost is paramount.

A significant breakthrough in this field is represented by the Carrera Unified Formulation (CUF) [26], a versatile mathematical framework capable of integrating both low-fidelity (ESL and LW) and high-fidelity (CW) theories into a single formulation. CUF is based on the concept of a fundamental nucleus that allows for a compact expression of the structural problem. This hierarchical characteristic permits a gradual enhancement of the model's level of detail, transitioning from a simplified representation to a comprehensive description of the structural behaviour without the need to rebuild the model from scratch with each increase in complexity. Consequently, CUF offers considerable advantages in terms of flexibility and computational efficiency, enabling the selection of the most appropriate fidelity level according to the specific analytical requirements and facilitating a systematic comparison of the modal predictions obtained using different approaches.

Despite the numerous studies and existing implementations, a significant research gap remains in the comparative evaluation of the different modelling theories applied to sandwich panels with honeycomb cores, particularly regarding their ability to accurately reproduce the modal responses. On one hand, homogenization-based theories are effective in providing a global overview of the structural dynamics; on the other hand, these may neglect local effects that could play a critical role under specific operating conditions. This limitation has raised the question of how much the simplifications in the ESL and LW models impact the accuracy of modal predictions compared to a more detailed CW model and how CUF might effectively bridge the gap between different fidelity levels.

The present study aims to address this gap by offering a comparative analysis of the three modelling methodologies, ESL, LW, and CW, within the CUF framework, with particular attention to the linear modal response of sandwich structures with honeycomb cores. The objectives are twofold: firstly, to evaluate the accuracy and predictive capability of each approach in reproducing the natural frequencies and mode shapes, highlighting the differences and potential limitations associated with each simplification; secondly, to demonstrate how the adoption of CUF can overcome the limitations of homogenized models while concurrently reducing the computational cost relative to traditional high-fidelity models, such as those based on 3D finite element methods. The novelty of this study lies in the proposal of an integrated methodology that exploits the potential of CUF to systematically compare models of varying fidelity, while providing a critical discussion of the trade-offs between precision and computational efficiency. The work provides a systematic assessment of the dynamic response of sandwich panels with honeycomb cores by comparing three CUF-based incremental modelling fidelities; the study offers a reference outline, highlighting the effects of model simplifications on frequency prediction and mode representation. This work provides a systematic CUF-based comparison across ESL, LW, and CW formulations for honeycomb sandwich plates in free vibration. The study addresses higher-order modes and local core effects, and employs MAC-based mode pairing to ensure consistent cross-model matching. The results highlight the outstanding capability of CW models in accurately capturing local and high-frequency phenomena, thus demonstrating their unique potential for realistic sandwich applications. The analysis clarifies the cost-accuracy trade-off among the three formulations within a single, coherent framework. This research paves the way for a more informed and targeted use of different modelling theories, fostering a better integration between high-fidelity analytical tools and simplified approaches, and highlighting the efficiency of CUF framework in these applications.

2. Methodology

The modelling of honeycomb sandwiches requires simplifications that adequately represent the underlying physics without sacrificing accuracy. The concept of multi-fidelity emerges as an approach that integrates models of varying complexity and accuracy to balance computational efforts and solution accuracy. By tailoring the fidelity level to the specific characteristics of the problem and the desired results, this method allows for efficient resource use while maintaining appropriate precision. For instance, lower-fidelity models can provide quick insights into global behaviour, while higher-fidelity models are applied to critical regions to ensure more accurate predictions, balancing computational cost with the required level of detail. These simplifications form the basis of Equivalent Single Layer, Layer-Wise, and Component-Wise theories, which offer varying degrees of fidelity in representing thickness and interlayer interactions. The Carrera Unified Formulation is adopted in this work as it provides a unified and hierarchical framework that allows ESL, LW, and CW models to be consistently formulated and directly compared within the same theoretical and numerical framework. In the following subsections, a description of these theories is provided, together with a comparative assessment of their limitations and capabilities.

2.1. Carrera unified formulation

The Carrera Unified Formulation stands out as a versatile and efficient mathematical framework capable of representing ESL, LW, and CW theories under a single formulation. CUF employs a compact notation to express displacement, strain, and stress fields across all theories. By introducing the concept of the fundamental nucleus, CUF reduces the governing equations of the problem into a minimal set of building blocks that are independent of the order of expansion or the theory adopted. One of CUF's main advantages is its hierarchical approach: by adjusting the order of the expansion, it is possible to transition between low-fidelity ESL models and higher fidelity LW or CW representations. This

flexibility allows engineers to select the most appropriate model based on accuracy requirements and computational resources. In the following, the CW representation and modeling of the sandwich structure with honeycomb core that is object of the present study is described. The CUF-based structural modelling method allows for the accurate representation of complex geometries as 1D elements, addressing the computational cost of traditional 3D or 2D finite element methods. Classical 1D beam models, though efficient, cannot capture detailed mechanical behaviour in complex structures. CUF overcomes this by incorporating high-order Lagrange polynomials for cross-sectional discretization, refining both geometry and structural response. In beam theory, the beam axis typically corresponds to the largest dimension, with the transverse dimensions defining the cross-sectional shape, see Fig. 1. On the other hand, CUF introduces an innovative approach where the beam axis can be reoriented, allowing cross-sectional details to be directly included in the mathematical model. The axis can extend transversely rather than along the structure's predominant dimension, offering flexibility in beam modelling selection, see Fig. 1.

The following sections detail the implementation of ESL, LW, and CW approaches employing CUF-based beam modelling.

2.2. Theories based on core homogenization

The structural analysis of sandwich panels with honeycomb cores is often approached using homogenization techniques, which simplify the complex structure of the core material into equivalent macroscopic properties. Lower-fidelity theories, such as the ESL and LW approaches, are built upon this framework.

2.2.1. Honeycomb equivalent mechanical properties

The concept of homogenization involves replacing the periodic cellular structure with an equivalent orthotropic continuum material, which replicates the macroscopic response of the core. A reference extensive description of cellular structures, involving also the mechanical properties homogenization is provided in ref., [27]. Some general reviews on the topic are available in refs., [28,29]. In general, there are different possible homogenization techniques, based on analytical [30–32], numerical [33,34], or experimental [35,36] approaches. One of the most adopted, for its generalizable application and easiness to be implemented, is the technique based entirely on analytical approaches, exploiting the strain-energy principles to determine the orthotropic elastic constants of honeycomb cores. By employing Castigliano's second theorem considering a representative cell element (RCE), it is possible to derive closed-form expressions for in-plane and out-of-plane moduli, shear moduli, and Poisson's ratios. These derivations relied on the proper definition of the RCE, a periodic unit of the honeycomb structure, and accounted for axial and bending deformations while neglecting minor contributions such as shear deformation in inclined walls. The work proposed in ref., [37] is notable for its analytical rigor and practical relevance. The study demonstrated that the equivalent properties could be expressed as functions of the honeycomb's geometric and material parameters, such as wall thickness, cell angle, and relative density. The resulting formulae provide a comprehensive and efficient tool for predicting the structural behaviour of honeycomb-core sandwich panels without resorting to finite element models, which are computationally expensive for such detailed geometries. The accuracy of this approach was validated by comparing the analytical results with experimental and numerical data from the literature, showcasing a good agreement. Fig. 2 represents the representative cell element of a general honeycomb core; main dimensions are indicated in the figure, i.e., thickness t, edge length l, cell height h, and internal angle θ.

Following the formulation proposed in ref., [37], Eqs. (1–9) are obtained to compute the equivalent mechanical properties of the homogenized core, namely, in plane elastic moduli, E_x and E_y, out of plane elastic modulus E_z, Poisson ratios ν_{xy}, ν_{xz}, ν_{yz}, in plane shear modulus G_{xy}, and out of plane shear moduli G_{xz} and G_{yz}. Finally, also the equivalent density of the homogenized core can be derived by means of Eq. (10). In the following equations, E_m, ν_m, G_m and ρ_m are the elastic modulus, the Poisson ratio, the shear modulus, and the density of the honeycomb base material, respectively. All the details of the derivation of equivalent elastic properties are available in ref., [37].

- ***In-plane and out-of-plane elastic moduli***

$$E_x = \frac{E_m\left(\frac{t}{l}\right)\cos\theta}{\left(\frac{h}{l}+\sin\theta\right)\left[\cos^2\theta+\left(\frac{l}{t}\right)^2\sin^2\theta\right]} \tag{1}$$

$$E_y = \frac{E_m\left(\frac{t}{l}\right)\left(\frac{h}{l}+\sin\theta\right)}{\cos\theta\left[\sin^2\theta+\left(\frac{l}{t}\right)^2\cos^2\theta\right]} \tag{2}$$

$$E_z = E_m\left(\frac{t}{l}\right)\frac{\left(1+\frac{h}{l}\right)}{\cos\theta\left(\frac{h}{l}+\sin\theta\right)} \tag{3}$$

- ***Poisson's ratios***

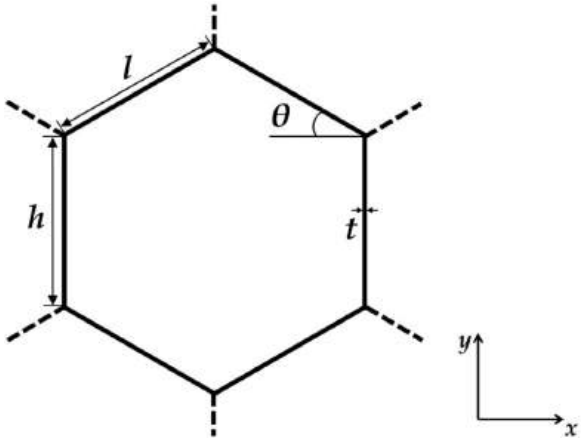


Fig. 2. Honeycomb core representative cell element (RCE).

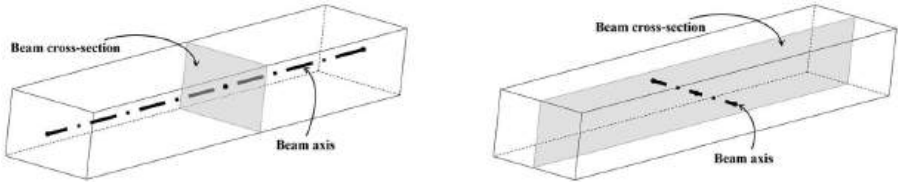


Fig. 1. Conventional (left) and novel (right) beam representations.

$$\nu_{xy} = \frac{sin\theta\left[1+\left(\frac{l}{t}\right)^2\right]}{\left(\frac{h}{l}+sin\theta\right)\left[1+\left(\frac{l}{t}\right)^2 tan^2\theta\right]} \tag{4}$$

$$\nu_{xz} = \nu_m \frac{E_x}{E_z} \tag{5}$$

$$\nu_{yz} = \nu_m \frac{E_y}{E_z} \tag{6}$$

- ***In-plane and out-of-plane shear moduli***

$$G_{xy} = E_m\left(\frac{t}{l}\right)^3\left(\frac{l}{h}\right)^2 \frac{\left(\frac{h}{l}+sin\theta\right)}{cos\theta\left(1+\frac{h}{4l}\right)} \tag{7}$$

$$G_{xz} = G_m\left(\frac{t}{l}\right)\frac{cos\theta}{\left(\frac{h}{l}+sin\theta\right)} \tag{8}$$

$$G_{yz} = G_m\left(\frac{t}{l}\right)\frac{\left(\frac{h}{l}+sin\theta\right)}{cos\theta\left(1+\frac{h}{l}\right)} \tag{9}$$

- ***Equivalent density***

$$\rho = \rho_m\left(\frac{t}{l}\right)\frac{\left(1+\frac{h}{l}\right)}{cos\theta\left(\frac{h}{l}+sin\theta\right)} \tag{10}$$

2.2.2. Equivalent single layer theory

The Equivalent Single Layer theory is a simplified approach where the entire multilayered structure is treated as a single homogeneous layer. This simplification is particularly useful for global analyses, where capturing the overall behaviour of the structure is more important than addressing local effects. ESL approach drastically reduces computational costs by limiting the number of variables needed to describe the structure's mechanics.

In ESL theories, the displacement fields are expanded along the thickness direction z using a predefined set of basis functions. In general, for ESL models, the displacement fields are expressed as in Eq. (11):

$$u(x,y,z) = F_\tau(x,z)u_\tau(y),\ \tau = 0,1,..,N \tag{11}$$

where $u(x,y,z)$ is the displacement field and $F_\tau(x,z)$ are the expansion functions of order N. For a first order Taylor expansion, i.e. $N = 1$, it results as provided by Eq. (12):

$$\begin{aligned} u_x(x,y,z) &= u_{x1}(y) + x\,u_{x2}(y) + z\,u_{x3}(y) \\ u_y(x,y,z) &= u_{y1}(y) + x\,u_{y2}(y) + z\,u_{y3}(y) \\ u_z(x,y,z) &= u_{z1}(y) + x\,u_{z2}(y) + z\,u_{z3}(y) \end{aligned} \tag{12}$$

Higher-order functions could allow to improve the model resolution. This formulation allows for capturing the effects of bending and transverse shear with a reduced number of degrees of freedom. However, it does not explicitly account for displacement and stress variations between individual layers. The ESL theories hence present a number of unknown variables that are independent of the number of the structure's layers.

2.2.3. Layer-wise theory

The Layer-wise theory addresses the limitations of ESL models by introducing independent displacement variables for each layer of the structure. However, this increased fidelity comes at the cost of greater computational effort, as the number of degrees of freedom increases with the number of layers. The mechanical properties for this theory are homogenized by considering each layer independently. In the LW theory, the displacement fields are expressed as in Eq. (13):

$$\boldsymbol{u^k} = F_\tau\,\boldsymbol{u^k_\tau},\ \tau = 1,2,\ldots,N \tag{13}$$

where expansion functions F_τ are now Lagrange polynomials defined at the k-layer level; k is hence the number of layers. Also in the LW case, the model can be expressed for a general N-order Lagrange expansion, by adding higher-order terms, as in Eq. (14):

$$\begin{aligned} u^k_x(x,y,z) &= F_1(x,z)u^k_{x1}(y) + F_2(x,z)u^k_{x2}(y) + \ \ldots\ldots + F_N(x,z)u^k_{xN}(y) \\ u^k_y(x,y,z) &= F_1(x,z)u^k_{y1}(y) + F_2(x,z)u^k_{y2}(y) + \ \ldots\ldots + F_N(x,z)u^k_{yN}(y) \\ u^k_z(x,y,z) &= F_1(x,z)u^k_{z1}(y) + F_2(x,z)u^k_{z2}(y) + \ \ldots\ldots + F_N(x,z)u^k_{zN}(y) \end{aligned} \tag{14}$$

Accordingly, a graphical representation of the definition of the skins and homogenized core is reported in Fig. 3, taking into a account a $N = 9$ Lagrange expansion.

Compared to ESL models, the LW theory improves the representation of stress distributions and allows for capturing local intralayer phenomena. Fig. 4 represents qualitatively the displacement field of a multilayered structure, described by the ESL and LW approaches. LW approaches increase the resolution of the displacement field and are able to detect local effects, but these requires computational resources proportional to the number of layers. However, also for LW models an homogenization of the mechanical properties is required, at a layer level in this case.

2.3. Component-wise modelling

Component-Wise theories take fidelity to the highest level by modelling each structural component, such as the core and skins in a sandwich structure, as an independent subdomain. Hence, no homogenization or simplification of the structure is required. This approach is particularly advantageous for capturing complex interactions between components with highly different mechanical properties, such as anisotropic cores and stiff face sheets. CW representation does not need any simplification or homogenization of the multi-layered structures, as it allows a precise modeling of the actual geometry of the structure.

In this CW formulation, hence, the sandwich structure is modelled by means of 1D beam elements; the beam axis is aligned with the honeycomb thickness, see Fig. 5.

The cross-sections of the skins and honeycomb core are discretized using high-order Lagrange polynomials. This means that the cross-section is represented by a layout of Lagrange points arranged into proper

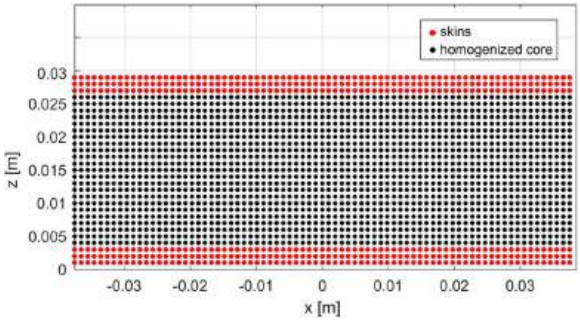


Fig. 3. Lagrangian discretization of skins and homogenized core for LW modelling.

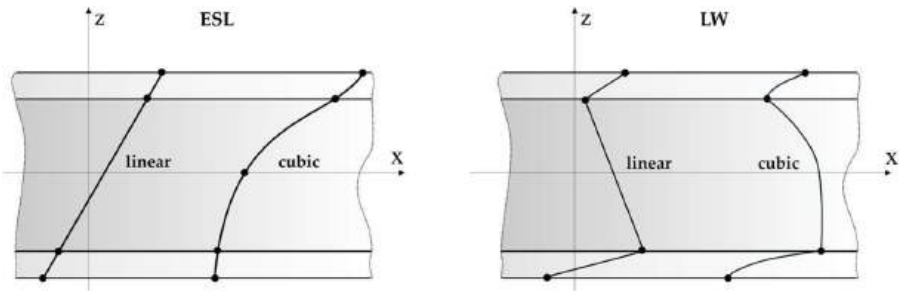


Fig. 4. ESL (left) and LW (right) qualitative displacement field, for linear and cubic cases, indicating the increased resolution of LW approach. Image adapted from ref., [38].

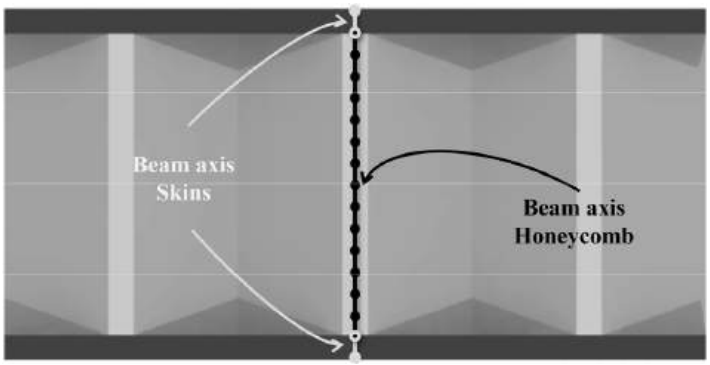


Fig. 5. Beam axis of the sandwich structure. The beam axis follows the thickness of the panel.

subdomains. The three-dimensional displacement field is obtained by interpolating the displacements evaluated at the Lagrange points. The interpolation order is determined by the number of points used: four Lagrange points (L4) provide a bilinear isoparametric interpolation, nine points (L9) a quadratic one, and 16 points (L16) a cubic one. The total number of degrees of freedom equals the sum of the displacement components associated with all the Lagrange points used. For example, the interpolation functions for a L9 expansion are:

$$
\begin{aligned}
F_\tau &= \frac{1}{4}\left(r^2 + rr_\tau\right)\left(s^2 + ss_\tau\right)\tau = 1,3,5,7 \\
F_\tau &= \frac{1}{2}s_\tau^2\left(s^2 + ss_\tau\right)\left(1 - r^2\right) + \frac{1}{2}r_\tau^2\left(r^2 + rr_\tau\right)\left(1 - s^2\right)\tau = 2,4,6,8 \\
F_\tau &= \left(1 - r^2\right)\left(1 - s^2\right)\tau = 9
\end{aligned}
\tag{15}
$$

where r_τ and s_τ are the coordinates of the nine Lagrange points and r and s vary from -1 to $+1$. Full details are provided in ref., [26]. As for the LW, also in the CW theory the displacement field can be expressed as in

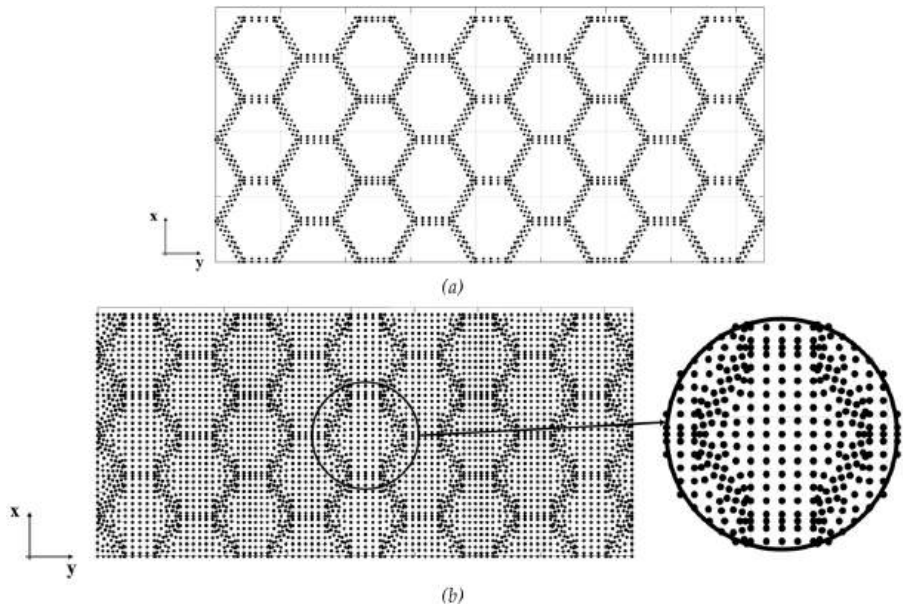


Fig. 6. Lagrangian discretization of: (a) honeycomb core; (b) skin. The Lagrangian points shared between skin and core, which ensure kinematic continuity, are visible.

Eq. (13), but in this case the k-th index represent the k-th component of the structure. A key difference in the present CW modelling, as previously described, lies in the definition of the sandwich cross-section and in the related beam axis. In this case, hence, the displacement filed described by N-order Lagrange expansions, is rewritten as in Eq. (16):

$$\begin{aligned} u_x(x,y,z) &= F_1(x,y)u_{x1}(z) + F_2(x,y)u_{x2}(z) + \ ..... + F_N(x,y)u_{xN}(z) \\ u_y(x,y,z) &= F_1(x,y)u_{y1}(z) + F_2(x,y)u_{y2}(z) + \ ..... + F_N(x,y)u_{yN}(z) \\ u_z(x,y,z) &= F_1(x,y)u_{z1}(z) + F_2(x,y)u_{z2}(z) + \ ..... + F_N(x,y)u_{zN}(z) \end{aligned} \tag{16}$$

where the section expansion function are defined in the x-y plane, see Figs. 6 and 7, whereas the beam axis is defined parallel to the z-axis, directed along the thickness of the sandwich, as represented in Fig. 8. To maintain displacement continuity at their interfaces, shared Lagrange points are defined. This ensures compatibility of displacements and strains between the skins and the honeycomb core, preserving interface continuity. The skin discretization must incorporate these common points, preventing discontinuities. The accurate alignment of shared Lagrange points allows the proper coupling between the skins and core, as illustrated in Fig. 6, ensuring precise interface representation.

For all the representations, the displacement field is then discretized along the defined beam axis by means of a Finite Element approximation, as reported in Eq. (17):

$$\boldsymbol{u}_\tau(y) = N_i(y)\boldsymbol{q}_{\tau i} \ i = 1, 2, ...N \tag{17}$$

where N_i are the shape functions representing the beam axis, and $\boldsymbol{q}_{\tau i}$ are the nodal unknowns. By merging this approximation within the full expression of the displacement field, and the virtual variation of the field is written as in Eq. (18):

$$\delta\boldsymbol{u}(x,y,z) = F_s(x,z)N_j(y)\delta\boldsymbol{u}_{js} \ s = 1, 2, ..., M \ j = 1, 2, ...N \tag{18}$$

The assembled models built according to CUF-based LW and CW representations, are hence represented as schematically shown in Figs. 7 and 8, respectively. A simplified CW representation is provided in Fig. 9, replacing the plotting of the actual nodes with uniform cross-sections, to provide an easier-to-read graphical representation. The modelling workflow is solver-agnostic and formally identical for all CUF formulations; it consists of two steps: (i) generation of the CUF section mesh; (ii) definition of the beam axis and its axial discretization. In step (i), the section mesh generation procedure is the same, but in light of the different logic used to model the beam, the section geometry differs across models: LW/ESL adopt a simple rectangular section representing transversal section of the homogenized panel (see Fig. 3), whereas CW meshes represent the actual longitudinal sections of skins and honeycomb core (see Fig. 6). Also in step (ii), the same operations are performed in all cases; only the selection of the beam axis orientation changes: for LW/ESL the beam axis is aligned with the axial direction of the panel, while for CW it is aligned with the thickness. No additional modelling steps or special treatments are required for CW model: interface compatibility is naturally handled by coincident section nodes, and the assembly-solution pipeline is the same for ESL, LW, and CW. As a result, CW does not add procedural complexity; it simply relies on a richer section geometry definition, which is precisely what enables its higher fidelity and accuracy highlighted in the results section.

Finally, the different 3D representations of the modelling of a honeycomb sandwich by means of the three theories, i.e., ESL, LW, and CW, are reported in Fig. 10. Regarding theory implementation into a software tool, it is relevant to highlight that all CUF-based models (ESL, LW, CW) were implemented and executed using an in-house research code developed by the authors' research group MUL2. The code provides a full implementation of the CUF framework, including preprocessing features, as section mesher and beam definition, assembly routines for the global K and M matrices, complete CUF-based theoretical implementation and solver. No commercial structural solver is used to produce the CUF results; commercial FE packages were employed only to compute the independent 3D reference solutions for comparison and validation purposes. This self-contained tool natively implements the original CUF theory within a single modular environment, which is a distinctive aspect of the approach.

The main geometric features of the honeycomb cell studied in this work, referring to Fig. 2, are $h = 11.65$, $l = 14.17$, and $\theta = 55°$; core thickness is equal to 2 mm, and skin thickness is equal to 0.5 mm. The modal analysis have been performed considering the plate clamped at one edge and free at the other. The reference sandwich plate considered in the numerical tests has the following dimensions: length equal to 170 mm, width equal t 75 mm, and height equal to 28 mm. Both face sheets and core are made of aluminium, with elastic modulus $E = 70$ GPa, Poisson's ratio $\nu = 0.33$, and density $\rho = 2700$ kg/m^3. The homogenised core for ESL and LW models has equivalent elastic properties obtained via analytical homogenization and reported in Table 1.

2.4. Governing equations

The governing equations are derived from the virtual work principle, see Eq. (19), which states that the sum of the virtual variations of internal strain energy (δL_{int}) and external load work (δL_{ext}) is equal to zero for each infinitesimal arbitrary virtual displacement, as:

$$\delta L_{int} - \delta L_{ext} = 0 \tag{19}$$

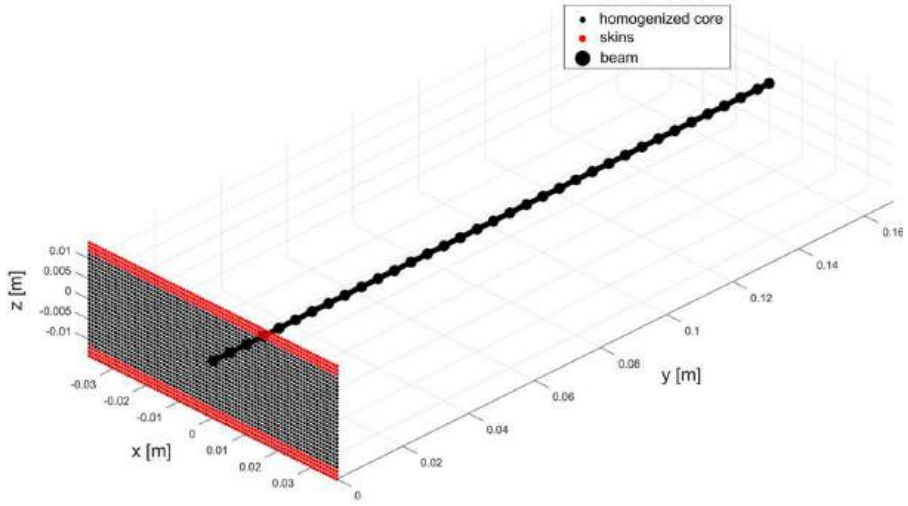


Fig. 7. Scheme of the LW modelling of the sandwich structure. The beam axis follows the panel's length.

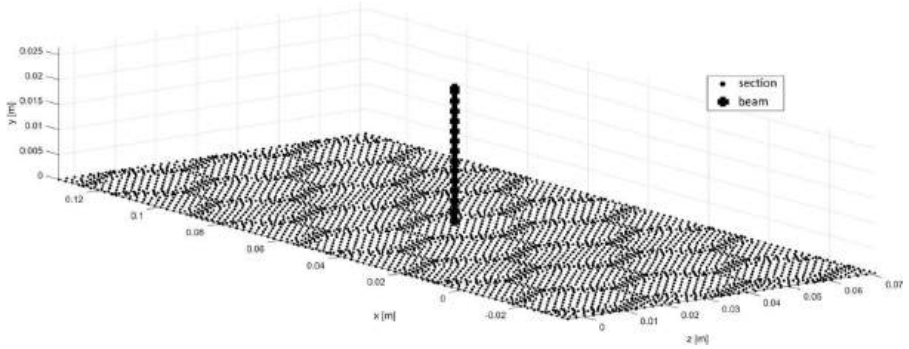


Fig. 8. Scheme of the CW modelling of the sandwich structure. The beam axis follows the panel's thickness.

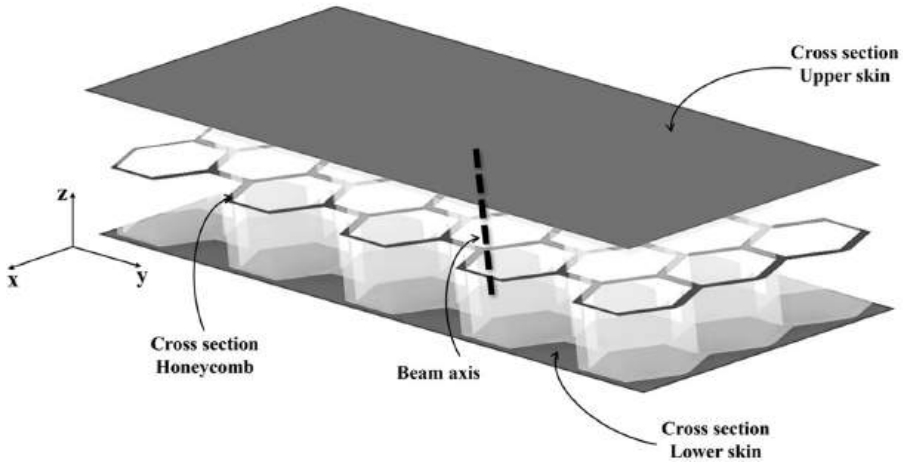


Fig. 9. Qualitative scheme of the CW modelling of the sandwich structure.

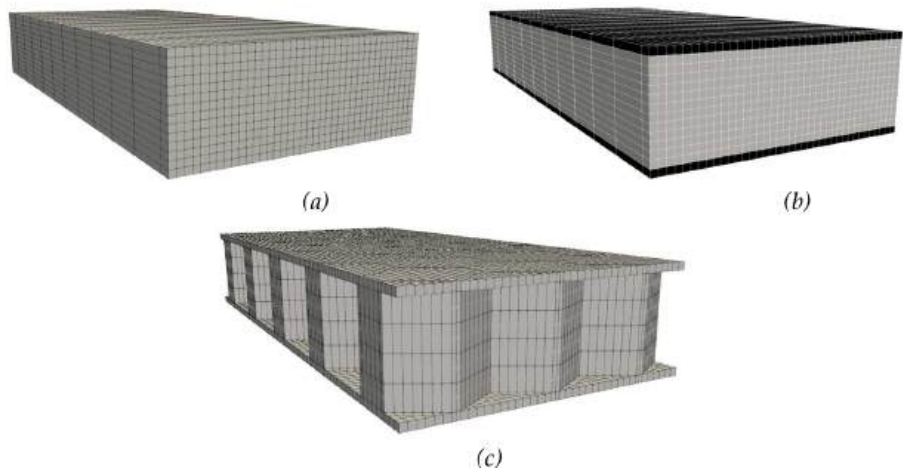


Fig. 10. Different modelling of the sandwich structure: (a) ESL, (b) LW, (c) CW.

Table 1
Equivalent mechanical properties for the honeycomb core.

Model	E_x [MPa]	E_y [MPa]	E_z [MPa]	G_{xy} [MPa]	G_{xz} [MPa]	G_{yz} [MPa]	ν_{xy}	ν_{xz}	ν_{yz}
Kumar	1645	101	19,123	691	1282	5763	0.25	1.7×10^{-3}	2.8×10^{-2}

The term δL_{int}, representing internal virtual work, is the virtual variation of the internal strain energy, considering a structure subjected to a virtual displacement; the latter is compatible with the geometric constraints. Consequently, this can be defined as in Eq. (20):

$$\delta L_{int} = \int_V \delta \boldsymbol{\varepsilon}^T \boldsymbol{\sigma} \, dV \tag{20}$$

where $\boldsymbol{\varepsilon}$ and $\boldsymbol{\sigma}$ are the strain tensor and the stress tensor, respectively; V is the volume domain volume. In the vectorial representation of Eq. (21), $\boldsymbol{\varepsilon}$ and $\boldsymbol{\sigma}$ are correlated as:

$$\boldsymbol{\varepsilon} = \boldsymbol{D}\boldsymbol{u} \tag{21}$$

where $\boldsymbol{D}$ is strain-displacement matrix, which is a linear operator containing the partial derivatives of the displacement components. To complete the problem, the correlation between stresses and strains is given by the Hooke's law, see Eq. (22), considering isotropic material:

$$\boldsymbol{\sigma} = \boldsymbol{C}\varepsilon \tag{22}$$

where $\boldsymbol{C}$ represents the stiffness matrix. Properly combining the relations of Eqs. (17,18,21,22), the equation in Eq. (18) is rewritten in the new form of Eq. (23):

$$\delta L_{int} = \delta \boldsymbol{u}_{js}^T \boldsymbol{K}^{ijrs} \boldsymbol{u}_{ir} \tag{23}$$

where $\boldsymbol{K}^{ijrs}$ is the 3×3 fundamental nucleus of the stiffness matrix; a complete derivation of fundamental nuclei is available in ref., [26]. Finally, the dynamic problem, neglecting the structural damping, can be expressed as in Eq. (24):

$$\boldsymbol{M}\ddot{\boldsymbol{q}} + \boldsymbol{K}\boldsymbol{q} = 0 \tag{24}$$

and solving the following eigenvalues problem of Eq. (25):

$$\left(\boldsymbol{K} - \omega_k^2 \boldsymbol{M}\right)\boldsymbol{q}_k = 0 \tag{25}$$

the k-th natural frequency ω_k^2 and eigenvector $\boldsymbol{q}_k$ can be computed. The generalized eigenvalue problem in Eq. (25) was solved in the framework of a linear undamped modal analysis. The stiffness and mass matrices, assembled according to each CUF formulation (ESL, LW, CW), were supplied to an eigensolver to compute the required set of eigenpairs. Implicitly Restarted Arnoldi Method (IRAM) is the method used for computing eigenvalues and corresponding eigenvectors; it is an algorithm widely used for solving large-scale, sparse eigenvalue problems. It is designed for matrices where a direct application of the entire matrix is too computationally expensive, relying on a reverse interface that requires user-provided matrix-vector products instead of the full matrix. IRAM algorithm is widely used to solve these problems and it is integrated into many common structural computing codes. The eigenvectors are mass-normalized and the corresponding natural frequencies are sorted in ascending order. The number of computed modes was selected to include both the global and the higher-frequency local responses discussed in Section 3.

2.4.1. Benchmark study case

Literature references are considered to preliminarily assess the accuracy of the representations of multilayered structures by means of the different theories adopted in this study. Benchmark cases of sandwich structures are analyzed, and the outcomes of linear static analyses are compared. Regarding the LW model, the reference proposed in ref., [39], and discussed in ref., [40], is considered; a representation of the geometry and the applied loading condition of this benchmark is provided in Fig. 11. In the reference work the problem is solved using plate formulation, whereas in the present work one-dimensional beam finite elements are employed. The sandwich structure is characterized by skins of different thickness, 0.1 mm and 0.5 mm for top and bottom, respectively. The structure is simply supported at four bottom edges, and loaded with uniform pressure on the top skin. The width, length, and height are 100 mm, 200 mm, and 12 mm, respectively. Skins are made in aluminum, whereas the core homogenized properties are directly given in ref., [40], namely: $E_x = E_y = 3.0$ MPa, $E_z = 2.8$ MPa, $E_{xz} = E_{xy} = E_{yz} = 1.0$ MPa, $\nu = 0.25$. The results in Table 2 show good agreement in terms of displacement and stress, supporting the reliability of the current implementation of the LW theory for the modeling of sandwich structures.

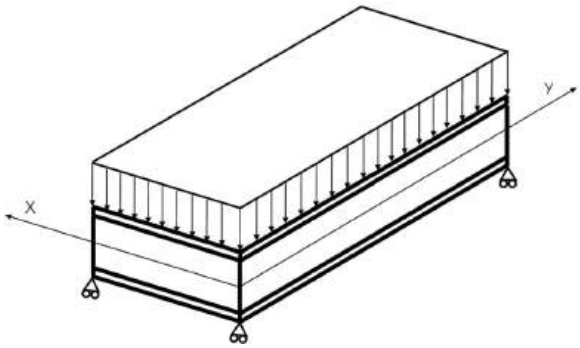


Fig. 11. Reference benchmark for LW assessment. Image adapted from ref., [40].

The assessment of the static response of the CW theory proposed in the present study has already been investigated in ref., [41]. Specifically, in ref., [41] the accuracy of the CW approach for honeycomb sandwich is proven for different loading conditions, providing also a detailed focus on the through-the-thickness stress prediction capability of the CW representation.

To further assess the validity of the CW approach, a comparison against a benchmark sandwich honeycomb in terms of modal response has been performed. As a reference, we selected the case reported in ref., [42], where the modal analysis of the proposed sandwich panel is stated to have been validated by experimental tests; this benchmark was therefore considered particularly suitable for our purposes. The honeycomb sandwich panel used in the benchmark has the following dimensions: length 330 mm, width 40 mm, total height 23 mm, core height 22 mm, and skin thickness 0.5 mm. The hexagonal unit cell is regular, with side length 3.65 mm and wall thickness 0.09 mm. The reference model also includes an adhesive layer between the hexagonal cells with a thickness of 0.06 mm. In our model, this layer was neglected to simplify the modeling without reasonably compromise the overall result. The two reference models of the sandwich beam are shown in Fig. 12.

Table 3 reports the comparison between the modal analysis results provided by the benchmark and those obtained with the CUF CW approach for the first three modes, as proposed in ref., [42]. The data show close agreement between the CW model and the validated 3D FEM results of ref., [42], both in terms of mode shapes and natural frequencies. The minor overestimation of the frequencies can be attributed to the omission of the adhesive layer, which slightly increased the overall stiffness of the structure. Overall, the results provide solid confirmation of the predictive capability of the CW model.

Table 2
Comparison of linear static results with literature benchmark.

	max u_z [mm]	
	Top face	Bottom face
LW	-0.411	-0.409
ref., [40]	-0.451	-0.448

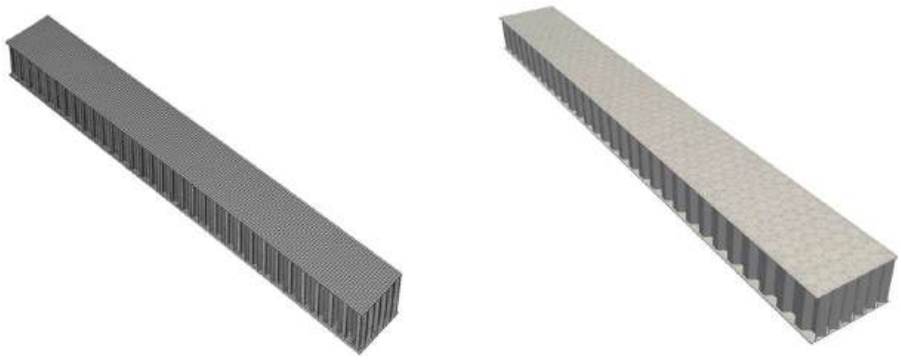
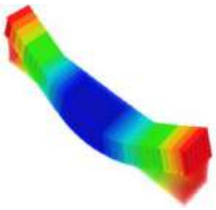
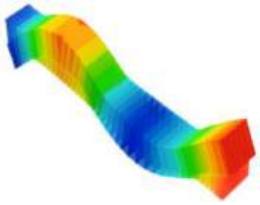
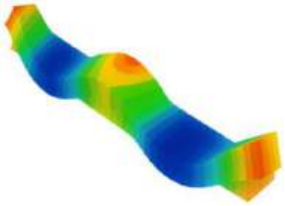


Fig. 12. 3D FE benchmark sandwich panel of ref., [42] (left) and its CW model (right).

Table 3
Comparison of mode shapes and frequencies between 3D FEM benchmark, taken from ref., [42] and its CUF CW model.

Description	3D FEM benchmark [42]	CUF CW
Single bending	 Mode 1 $f = 1.235$ kHz	 Mode 1 $f = 1.258$ kHz
	Δ % freq. mode 1= +1.8 %	
Double bending	 Mode 2 $f = 3.041$ kHz	 Mode 2 $f = 3.160$ kHz
	Δ % freq. mode 2= +3.9 %	
Triple bending	 Mode 3 $f = 5.377$ kHz	 Mode 3 $f = 5.577$ kHz
	Δ % freq. mode 3= +3.7 %	

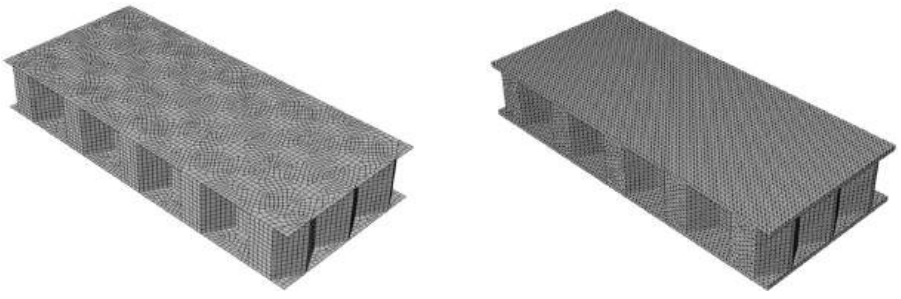


Fig. 13. 2D (left) and 3D (right) FEM mesh.

In Section 2.5, the results regarding modal response obtained with the different theories will be also compared with those obtained from commercial FEM models.

2.5. Comparison with FEM results

Finite element analyses on the sandwich structure test-case are performed using Abaqus to serve as a benchmark for comparing the CUF modelling results. Two FEM modelling strategies were adopted: a 2D shell-based and a 3D solid-based approach. In the 2D FEM modelling, Abaqus S4R quadrilateral shell elements were used to simulate the whole structure. In contrast, the 3D approach employed C3D10 quadratic elements to provide a more detailed structural response, accurately computing also through-thickness stresses. For both approaches, uniform mesh seed was applied for the entire structure; the mesh convergence analyses are reported in ref., [41]. At this stage, it has been decided that the whole sandwich structure is made by only one isotropic material, the aluminium. The main dimensions of the sandwich structure test-case are a width of 75 mm, a height of 28 mm, and a length of 170 mm. Fig. 13 shows the 2D and 3D FEM meshes, and Table 4 reports the comparison in terms of degree of freedom necessary to model the sandwich with the different approaches. For the CUF-based ESL model, a first-order Taylor expansion was adopted; the LW model employed a first-order layer-wise kinematic description. The CW model was formulated using a first-order Lagrange expansion by means of four-nodes L4 elements. The beam elements used are quadratic four-nodes B4 elements.

In all cases, convergence of natural frequencies was tested by mesh refinement. Specifically, for all CUF formulations, mesh refinement was conducted until the natural frequencies stabilized within a prescribed tolerance. Two refinement parameters were considered: (i) the axial discretization (number of and type of elements along the beam axis); (ii) the section discretization in terms of mesh density. The results for the CW case are reported in the following. Convergence was assessed on the first eight modes by monitoring the maximum relative change between successive refinements, and the final discretizations were selected once this change was considered acceptable respect to the variation of the computational effort. First, the beam refinement has been assessed, considering four different discretizations for the honeycomb core beam axis: (i) 2 B2 elements; (ii) 2 B4 elements; (iii) 4 B4 elements; (iv) 8 B4 elements. Results in terms of number of degree of freedom and percentage differences for the first eight eigenfrequencies with respect to the most refined case are reported in Table 5; the case with 4 B4 elements has been considered sufficiently refined for the present study.

Starting from the selected beam discretization, another level of mesh assessment has been performed, by considering the section spatial refinement. Three different cases have been considered, by using an average grid step for the whole section of 2 mm, 1.5 mm, and 1 mm, respectively. Results in terms of number of degree of freedom and percentage differences for the first eight eigenfrequencies with respect to the most refined case are reported in Table 6; the case with 2 mm mesh seed has been considered sufficiently refined for the present study. A same procedure has been applied to the ESL an LW models.

Although the selected benchmark involves a limited number of honeycomb cells, this configuration is chosen both for computational necessities and to underline the limits of classical homogenization techniques. In such compact configurations, the assumptions underlying equivalent models, such as sufficient representativeness, may be only partially satisfied, potentially affecting the accuracy of their predictions. This setup allows for a controlled evaluation of the predictive capabilities of simplified models and highlights the advantages of the CW formulation, which retains full geometric and mechanical detail without relying on homogenization assumptions.

The selected configuration is not intended to represent a specific practical application but rather to enable a controlled assessment of modelling fidelity. Its compact size allows the resolution of a wide modes range and the detection of local effects with a balanced computational effort. This information can be particularly relevant for benchmarking models applied to lightweight and stiff components such as aerospace structures operating in high-frequency regimes.

Table 7 reports the comparison of first ten natural frequencies computed by CUF-based ESL, LW, and CW theories, and those assessed by 2D and 3D FEM models, together with the percentage difference with respect to the 3D FEM, taken as reference. The structure is clamped in its root section, and no external loads are applied. The results in Table 7 demonstrate an excellent agreement between the natural frequencies computed with the CUF CW model and those obtained via the high-fidelity 3D FEM, despite the former needs only one-sixth of the degrees of freedom of the latter. In contrast, the lower-fidelity ESL and LW theories exhibit fluctuating accuracy compared to the more precise models. Moreover, it is plausible that a one-to-one correspondence between the mode shapes associated with the same natural frequency order may not always be possible. Consequently, it is necessary to perform a more thorough analysis of the outcomes derived from the ESL and LW models through a detailed comparison of eigenvalues and mode shapes with those obtained via the high-fidelity CW modelling. This discussion is presented in detail in the following section.

It is worth noting that the purpose of the present work is not to provide a further validation of the CUF approach itself, which has been widely assessed in the literature for both static and dynamic analyses of complex and multilayered structures. Instead, the focus here is to highlight how CUF-based models of different fidelity, i.e. ESL, LW, and CW, provide different levels of resolution in predicting the dynamic response, with particular emphasis on the limitations of homogenized

Table 4
Mesh sizes for the different models.

	Mesh seed	n° elements	n° nodes	DoFs
Mesh 2D	2 mm	14,833	14,218	**85,308**
Mesh 3D	2 mm	125,169	220,988	**662,964**
CUF ESL	–			**334**
CUF LW	–			**64,935**
CUF CW	–			**113,604**

Table 5
Mesh convergence results: beam refinement.

	2 B2	2 B4	4 B4	8 B4
DoFs	60,084	81,492	113,604	177,828
	|Δ%| freq.			
Mode 1	3.4	0.7	0.1	ref.
Mode 2	3.8	0.6	0.1	
Mode 3	3.7	0.4	0.1	
Mode 4	3.3	0.6	0.1	
Mode 5	1.8	0.4	0.0	
Mode 6	5.1	0.5	0.1	
Mode 7	3.7	0.3	0.2	
Mode 8	3.6	0.2	0.2	

Table 6
Mesh convergence results: section refinement.

	2 mm	1.5 mm	1 mm
DoFs	113,604	167,916	287,688
	|Δ%| freq.		
Mode 1	0.2	0.3	ref.
Mode 2	0.9	0.9	
Mode 3	0.5	0.4	
Mode 4	0.2	0.3	
Mode 5	0.9	1.0	
Mode 6	1.0	1.0	
Mode 7	0.3	0.3	
Mode 8	1.1	0.8	

Table 7
Comparison of the first ten natural frequencies computed via different models.

	CUF ESL		CUF LW		CUF CW		FEM 2D		FEM 3D	
	f [kHz]	Δ%	f [kHz]	Δ%	f [kHz]	Δ%	f [kHz]	Δ%	f [kHz]	Δ%
Mode 1	0.826	-10.1	0.832	-9.5	0.890	-3.1	0.898	-2.3	0.919	
Mode 2	1.306	-10.6	1.291	-11.7	1.421	-2.8	1.421	-2.8	1.462	
Mode 3	4.193	53.1	2.864	4.6	2.733	-0.2	2.715	-0.9	2.739	
Mode 4	4.579	9.6	4.386	5.0	4.223	1.1	3.982	-4.6	4.176	
Mode 5	4.342	-25.9	5.124	-12.6	5.789	-1.2	5.688	-2.9	5.861	ref
Mode 6	5.383	-9.2	5.173	-12.7	5.896	-0.5	5.742	-3.1	5.927	
Mode 7	11.147	38.9	8.188	2.1	8.015	-0.1	7.950	-0.9	8.022	
Mode 8	11.465	26.2	10.239	12.7	9.098	0.1	8.719	-4.0	9.085	
Mode 9	12.380	-0.7	10.754	-13.7	12.500	0.2	12.101	-2.9	12.468	
Mode 10	13.025	1.3	13.142	2.3	12.851	0.1	12.664	-1.4	12.847	

models and the potential of the CW approach in capturing local effects. For this purpose, a high-fidelity 3D FEM model was adopted as the reference solution. Such a choice is widely recognized in the literature as adequate for validating numerical models capable of representing the dynamic behaviour of sandwich structures.

3. Results

This section presents the primary findings of the study. First, in Section 3.1, a detailed evaluation and comparison of the natural frequencies and mode shape predictions is provided, providing insights on the consistency of the different modelling approaches. Then, in Section 3.2, an the Modal Assurance Criterion (MAC) is adopted as a tool to support the comparison of the modal response of the sandwich skins. These investigations frame the discussion about the accuracy and reliability of the different fidelity theories. The comparison involves the CUF-based ESL, LW, and CW models; the latter is taken as a high-fidelity reference. The skin of the analysed sandwich is reduced to 0.5 mm, to amplify local modal deformation that may occur for this type of structures.

3.1. Comparison of modal analyses results

This section provides a detailed discussion of the comparison of the

Table 8
Mode shapes and frequencies of the first bending modes.

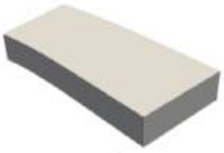
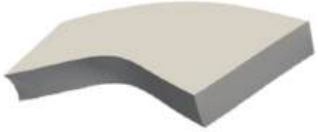
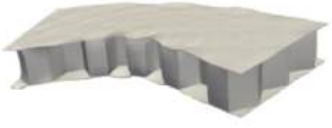
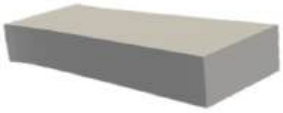
Description	ESL	LW	CW
Bending	 Mode 1 f=0.494 kHz	 Mode 1 f = 0.501 kHz	 Mode 1 f=0.621 kHz
In-plane bending	 Mode 2 f=0.898 kHz	 Mode 2 f=0.877 kHz	 Mode 2 f=1.026 kHz
Middle bending	 Mode 4* (3) f=2.909 kHz	 Mode 4 f=2.921 kHz	 Mode 4 f=3.321 kHz
In-plane middle bending	 Mode 6 f= 3.717 kHz	 Mode 6 f=3.549 kHz	 Mode 6 f=4.274 kHz

Table 9
Mode shapes and frequencies of the first torsional and extensional modes.

Description	ESL	LW	CW
Torsional	 Mode 3* (6) f=4.107 kHz	 Mode 3 f=2.007 kHz	 Mode 3 f=2.229 kHz
Extensional	 Mode 5* (4) f=3.106 kHz	 Mode 5 f=3.493 kHz	 Mode 5 f=4.210 kHz
Double torsion	 Mode 7* (11) f=12.302 kHz	 Mode 7 f=6.035 kHz	 Mode 7 f=6.655 kHz

sandwich modal outcomes achievable by ESL, LW and CW theories. To support the general and comprehensive discussion of the comparison of the modal analyses performed with different theories, mode shapes and natural frequencies are reported in Tables 8–12. For the sake of clarity in interpreting the results, the modes listed in the tables are arranged in ascending order based on the natural frequencies of the CW model, which serves as the reference. In cases where the ESL and LW outcomes do not exhibit a one-to-one correspondence with the CW modes, an star symbol is used to denote this discrepancy, and the actual order of the natural frequency is indicated in parentheses. The modal comparison among the ESL, LW, and CW theories highlights differences in natural frequencies and mode shapes, deriving from the simplifications introduced, i.e. core homogenization, hence from the differing assumptions regarding the distribution of stiffness and mass as well as local coupling effects. To start with the discussion of results, the initial focus is given to the modal analyses outputs relating the first six modes, reported in Tables 8 and 9, which can be defined as global modes. Among these two principal behaviors are detected: on the one hand, modes characterized by predominantly bending responses, and on the other, modes where torsional and extensional effects prevail. In the first group are modes 1, 2, 4, and 6, predominant bending behavior and a global structural response. Modes 1, 2, and 4, which are marked by out-of-plane and in-plane bending deformations, show agreement between the ESL and LW theories, with natural frequencies of 0.49 kHz and 0.50 kHz for mode 1, 0.89 kHz and 0.88 kHz for mode 2, and 2.91 and 2.92 for mode 4, respectively. In both cases, the CW theory leads to slightly higher values (0.62 kHz for mode 1, 1.03 kHz for mode 2, and 3.32 kHz for mode 4), suggesting that incorporating a more precise representation of the distribution of mass and stiffness, leads to an apparent increase in the structure's stiffness; however, the accuracy of lower fidelity theories seems still acceptable for these global modes. Similarly, mode 6, which involves an in-plane bending, follows the same trend: ESL and LW predict frequencies of 3.71 kHz and 3.55 kHz, respectively, while CW provides a higher estimate, 4.27 kHz. Here, the consistency between ESL and LW indicates that, for global deformations, the simplifications inherent in both models are adequate for reliable estimates, even though they do not fully capture the local contributions that, when included as in the CW theory, increase the effective stiffness. However, in a case as mode 4, if the thickness of the skins is increased from 0.5 mm to 2 mm, despite its global bending nature involving a central deformation, a slight decrease in frequency is observed (4.23 kHz in CW versus 4.57 kHz in ESL and 4.38 kHz in LW). This behavior may indicate that, under certain geometric and loading conditions, the influence of local contributions does not always reinforce the structure but can lead to a redistribution of the effective stiffness, thereby reducing its apparent value.

The second group comprises modes in which torsional and extensional effects dominate, as seen in mode 3 (predominantly torsional) and mode 5 (predominantly extensional). In mode 3, the ESL theory predicts a frequency of 4.11 kHz, which is significantly higher than those provided by LW (2.01 kHz) and CW (2.23 kHz). This notable overestimation by ESL may be attributed to its assumption of a homogeneous distribution of torsional stiffness, a simplification that fails to capture the true mechanical behavior arising from local effects. Accordingly, in mode 7 (double torsion), the ESL formulation predicts a frequency of 12.30 kHz, again a value significantly higher than the predictions provided by the LW (6.03 kHz) and CW (6.65 kHz) models. This supports the deduction that the ESL approach tends to overestimate the torsional stiffness by neglecting local cross-sectional deformability effects. Conversely, extensional mode 5 shows an opposite trend: ESL provides a lower estimate (3.11 kHz) compared to LW (3.49 kHz) and CW (4.21 kHz). This discrepancy suggests that, in the presence of an extensional response, the ESL simplification leads to an underestimation of the structure's resistance to deformation, whereas LW and, even more so, CW, are better able to assess the membrane behavior and the skin-core cells, resulting in a higher stiffness estimate. Also in this case, hence, it is not possible to conclude if generally a model can be more conservative than others, as the result strictly depends on the considered mode.

The discrepancies among the theories can be traced back to the different dealings of the coupling between local and global deformations and the underlying assumptions regarding the distribution of mass and

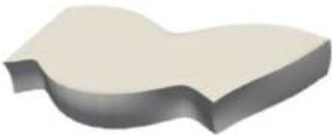
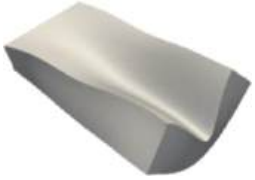
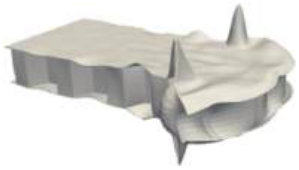
Table 10
Mode shapes and frequencies of the first modes with significant local effects - part 1. Each row summarizes the dominant deformation pattern; "missing mode" indicates that no match to the CW mode shape was found.

Description	ESL	LW	CW
Double bending	 Mode 8* (7) f=7.502 kHz	 Mode 8 f=7.426 kHz	 Mode 8 f=7.775 kHz
In-plane double bending	 Mode 9* (8) f=7.925kHz	 Mode 9 f=7.474 kHz	 Mode 9 f=9.094 kHz
Coupled bending-torsion	**missing mode** Mode / f=/	 Mode 10* (12) f=10.339 kHz	 Mode 10 f=11.072 kHz
Extension-shrinking	 Mode 11* (9) f= 9.111 kHz	 Mode 11* (10) f=10.033 kHz	 Mode 11 f=11.828 kHz
Bending with skin localized deformations	**missing mode** Mode / f=/	**missing mode** Mode / f=/	 Mode 12 f=12.405 kHz

stiffness. The ESL and LW theories, based on simplified models and a homogeneous representation of the core structure, are well suited for rapid and consistent estimations of global modes; considering the first modes, involving generally a global deformation shape, the results indicate that the ESL and LW theories are in close agreement for assessing global bending modes. However, these approaches may be limited when it is necessary to capture local deformations and complex interaction mechanisms, particularly in modes characterized by torsional and extensional responses. Although the CW theory requires greater modeling and computational complexity, it provides a more realistic description by reproducing local effects and leading to a more accurate prediction of the structure's natural frequencies.

The analysis of modes 8 through 12, represented in Table 10, introduces a new level of complexity compared to the previous cases, as these modes exhibit an overlap between global and local effects. This is particularly evident in the CW formulation, which identifies detailed deformation components that are absent or less pronounced in the ESL and LW models. The influence of such local effects is manifested both in a wider dispersion of natural frequency values among the different theories and in the emergence of modes that some models, such as ESL, fail to predict. Mode 8, a double bending mode with localized dimpling on the skins, shows a higher consistency between ESL (7.50 kHz), LW (7.42 kHz), and CW (7.77 kHz) predictions compared to torsional cases; nevertheless, by considering the mode shapes, CW still reveals a local deformation component that the two other models do not capture leading to a simplified mode description. In mode 9 (in-plane double bending), a more marked discrepancy is observed, with CW predicting a frequency of 9.09 kHz compared to 7.92 kHz for ESL and 7.47 kHz for LW. This suggests that CW captures additional local stiffness contributions, evidenced by the appearance of undulations on the structure's surfaces, which are only completely absent in LW and ESL. Mode 10, which involves a coupling between bending and torsion, is particularly

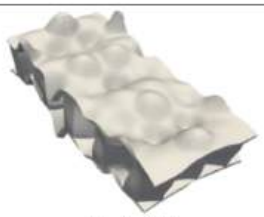
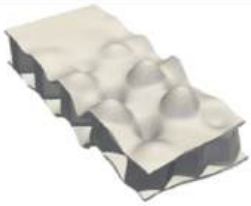
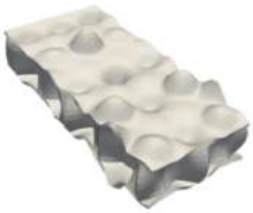
Table 11
Mode shapes and frequencies of the first modes with significant local effects - part 2 Each row summarizes the dominant deformation pattern; "missing mode" indicates that no match to the CW mode shape was found.

Description	ESL	LW	CW
Double in-plane bending with skin localized deformations	 Mode 10* $f = 11{,}186$ kHz	 Mode 11* $f = 10.272$ kHz	 Mode 13 $f = 12.499$ kHz
Double in-plane bending with skin localized deformations	 Mode 18* $f = 18.799$ kHz	 Mode 16* $f = 12.656$ kHz	 Mode 14 $f = 15.056$ kHz
Torsion and bending with skin localized deformations	**missing mode** Mode / $f = /$	**missing mode** Mode / $f = /$	 Mode 15 $f = 15.257$ kHz
Centreline bending with skin localized deformations	**missing mode** Mode / $f = /$	 Mode 13* $f = 10.907$ kHz	 Mode 16 $f = 15.320$ kHz
Tip-core extension	**missing mode** Mode / $f = /$	 Mode 14 $f = 11.419$ kHz	 Mode 17 $f = 16.017$ kHz

sensitive to local effects; considering the first twenty eigenvalues, ESL fails to predict this mode, at least within the first twenty roots, likely highlighting its limitations in capturing local-global interaction phenomena, whereas LW and CW identify the mode at frequencies of 10.33 kHz and 11.07 kHz, respectively. The higher stiffness indicated by CW implies that local effects not only exist but also play a significant role in reinforcing the system's dynamic behaviour. For mode 11 (shrinking-extension) ESL yields a frequency of 9.11 kHz for mode 11, while LW and CW provide higher values of 10.03 kHz and 11.82 kHz, respectively. In mode 12, i.e. a bending with pronounced local effects on the structure's skin, neither ESL nor LW can predict the eigenmode, indicating their inability to represent these local deformation phenomena, whereas CW identifies a frequency of 12.40 kHz. Overall, the absence of certain modes in the ESL and LW formulations underscores their limitations in modelling local deformations, local skin-core interaction, or local instability effects, particularly at higher frequencies, while the CW theory emerges as the most comprehensive approach for capturing significant local contributions.

Finally, it is interesting the analysis of modes at higher frequency with more accentuated local effects. The analysis of modes 13 to 17, see Table 11, shows that these are characterized by global deformations with a marked contribution from local phenomena; the CW theory, thanks to its high fidelity, delineates the displacement field of the entire structure in detail. It captures phenomena such as local indentations of the skin and specific deformations of the hexagons, features that are simplified or entirely neglected in homogenized models like ESL and LW. For instance, in mode 13 ESL estimates a frequency of 11.19 kHz and LW 10.27 kHz, while CW reaches 12.50 kHz. This increase should not be merely numerical: an analysis of the mode shapes shows that, unlike the solutions obtained with ESL and LW, CW reveals a more complex displacement field with localized sharp indentations in some of the transition zones between core and skin. Mode 14 further amplifies these differences. While ESL provides a frequency of 18.80 kHz and LW 12.66 kHz, CW estimates 15.06 kHz, a significant and opposite discrepancy with respect to the two lower fidelity models. The simplification inherent in homogenized models can lead to an overly idealized representation of the response, omitting local features that are potential linked to critical conditions. For the root 15, ESL and LW fail to identify

Table 12
High-frequency mode shapes with significantly relevant local effects.

CW		
 Mode 55 f=31.186 kHz	 Mode 66 f=33.448 kHz	 Mode 79 f=35.122 kHz
 Mode 84 f=35.377 kHz	 Mode 95 f=36.332 kHz	 Mode 99 f=36.825 kHz

the mode within the fist twenty eigenmodes, whereas CW detects it at a frequency of 15.26 kHz. The CW identifies a mode shape coupling bending and torsion and also showing localized deformations concentrated at junctions between hexagons, where the skin undergoes pronounced bending. These characteristics, cannot be detected at all by ESL formulation and are only partially modelled by LW, highlighting the need for high-fidelity models when a realistic evaluation of dynamic behaviour is required, especially in the presence of complex local effects. Mode 16 continues along the same lines: while ESL provides no estimate and LW identifies a frequency of 10.91 kHz, CW estimates the value at 15.32 kHz, accompanied by a mode shape that highlights deformations concentrated along the interaction zones between structural elements. In particular, CW shows that the displacement distribution along the interfaces between hexagons is not uniform but is characterized by peaks and undulations, indicating localized instabilities and significant variations in stiffness distribution. Finally, mode 17, a mode primarily involving the core deformation, and characterized by a significant extension of the terminal part of the structure, is detected by the CW theory, which estimates a frequency of 16.02 kHz, whereas a simplified mode shape is detected by LW model at a frequency of 11.419 kHz. Both mode shape and natural frequency underline the poor resolution of the LW in capturing this mode; being a core-related mode, and as this is not modelled as an independent layer in the ESL representation, ESL theory fails to detect this mode shape.

Overall, the analysis of high-frequency modes 13 to 17 demonstrates that homogenization-based theories cannot provide reliable estimates of natural frequencies and typically fail to capture the complexities of the displacement field, particularly regarding the description of skin dimpling and indentations, and hexagon local deformations. In contrast, the CW theory proves to be the most comprehensive tool, able to effectively detect global and local effects to offer frequency values that are more consistent with the actual structural stiffness, and detailed mode shapes, enabling a precise assessment of critical areas. This substantial difference in the ability to resolve local effects is crucial for applications where accurate modelling of vibrations and displacement distributions is essential for safety and design optimization, highlighting the importance of adopting high-fidelity models for the correct interpretation of the complex dynamic response of advanced multilayered structures.

The CUF framework is applicable for any geometry or boundary condition: ESL, LW, and CW are formulated and solved identically for any admissible honeycomb core shape or boundary condition. To keep the discussion focused on methodological aspects, the main text considers only a representative clamped-free case for a reference geometry. For completeness, Appendix A reports a summary of results for a honeycomb core with a smaller unit cell, and Appendix B reports the comparison for a different boundary condition, the clamped-clamped plate. The modelling workflow is unchanged and the same qualitative conclusions apply, indicating that the methodological approach is not tied to a specific mechanical set.

Besides accuracy, the computational cost of each formulation was also assessed. For this purpose, we considered the time required to extract the first 20 natural modes, running the analysis on a laptop having 16GB of RAM and a processor Intel Core i7-6700HQ CPU@2.60 GHz. The ESL model completed the analysis in approximately 83 s, while the LW and CW models required 657 s and 750 s, respectively. Although the CW formulation requires a moderately higher cost compared to ESL and LW, the additional effort remains acceptable and is well justified by the superior accuracy achieved, especially in capturing local dynamic effects. It is worth underlining that the comparison of computational times previously reported refer to the full pipeline of the in-house CUF code, which includes input parsing, boundary-condition setup, assembly of matrices, numerical solver, and output extraction. Such end-to-end timings are not expected to correlate directly with the number of DoFs, because they comprise substantial steps beyond the solver itself. It is also important to note that the in-house code has been developed for research purposes and could require implementation-level optimizations to achieve typical computational correlations obtained in commercial solvers.

To conclude this discussion on the potential capabilities of the different fidelity theories, a focus on some very-high frequency modes is provided. The high-frequency modes shown in Table 12 clearly demonstrate the unique capability of the CW theory to resolve extremely refined local details that are entirely beyond the reach of homogenized theories. At these frequencies, the dynamic behavior of the structure is dominated by local instability phenomena, with pronounced skin indentations and deformations concentrated also in correspondence of the individual hexagonal cells. The precision of the CW formulation not only

captures the spatial distribution of these deformations but also their interaction with the structure's internal geometry, an essential aspect for a realistic characterization of its vibrational behavior. The complexity of the mode shapes confirms that the dynamic response cannot be described solely in terms of global stiffness, but rather requires the ability to identify local effects, particularly in advanced configurations with cellular structures. This analysis underscores the importance of high-fidelity models for accurately predicting structural dynamic responses, especially in applications where high frequencies play a critical role in the design and reliability of the component. CUF-based CW description hence merges both the high-fidelity resolution of the vibrational analysis of complex structures, together with its exceptional flexibility in modeling and in the reduction of degrees of freedom needed to model the problem.

While the lower modes are typically dominant in the static and dynamic response of sandwich plates, the inclusion of higher-order modes in the present study is not merely of theoretical interest. In engineering practice, these modes may play a significant role in scenarios where the structural response is excited over a broad frequency spectrum. Examples include vibro-acoustic problems, where high-frequency modes govern sound transmission across lightweight panels, and aeroelastic or impact-related phenomena, where local deformations are activated at higher frequencies. Sandwich plates with honeycomb cores are often employed in aerospace applications specifically for their superior damping and insulation capabilities, properties that are directly linked to their behaviour in the high-frequency range. Therefore, providing an assessment of the accuracy of ESL, LW, and CW formulations at higher modal orders is crucial to demonstrate the potential of refined CUF-based models in capturing the full dynamic spectrum relevant to real-world applications. In this context, it is worth emphasizing that only the CW formulation proves capable of accurately resolving the complex deformation patterns associated with high-frequency phenomena, thereby offering the necessary predictive capability for engineering scenarios where such effects become critical.

It should be also noted that mesh refinement was applied consistently across the different CUF formulations to ensure numerical convergence. However, the discrepancies observed at higher frequencies are not related to discretization density but rather to the intrinsic modelling assumptions. In particular, the ESL and LW approaches rely on homogenized core descriptions, which inherently prevent the capture of local deformation patterns associated with short-wavelength modes. Conversely, the CW formulation, by explicitly resolving the core geometry, enables an accurate representation of these local effects, making it uniquely suited for analysing the high-frequency dynamic behaviour of sandwich structures. Finally, it is worth to underline that the computational time required to extract the first 99 modes was 3.2 times higher than that required to compute the first 20 modes.

3.2. Sandwich skins' modal assurance criterion

The aim of this section is to present an insight into the methodology used to compare the modal shapes obtained through the different methods. In fact, when studying such comparisons, on the one hand it is necessary to discuss the matching of the natural frequencies, given in the dedicated Table 7, and on the other hand a comparative study of the modal shapes of the skins is necessary in order to correctly associate the frequencies with their respective deformations. In the previous section, this comparison was supported by the individual discussion of each modal shape, and showed that the different models do not guarantee a direct one-to-one correspondence between the modes, giving justification for such differences. Therefore, the simple analysis of natural frequencies is not sufficient to evaluate the validity of comparisons of modal responses. One tool that can be coupled with such results is the Modal Assurance Criterion, which is a quantitative method of verifying the correlation between deformations obtained with different models or theories [43,44].

Given the complexity of the structure, and the different way it is modelled by the differing theories, it was decided to calculate the MAC for the sandwich skins only. Furthermore, considering the simplifications introduced in the ESL theory, for which it is not possible to isolate the skins, the comparison is carried out only for the LW and CW theories. MAC was computed according to its standard definition, as the normalized correlation between pairs of mode shapes. To ensure consistency, the eigenvectors from the different models were normalized and projected onto compatible degrees of freedom, so that the comparison was always carried out on matching displacement components. The process begins with the extraction of modal displacement fields from both the LW and CW models. In the LW formulation, the core is represented as an equivalent homogeneous layer; thus, the resulting nodal discretization and the corresponding modal displacements for the skins differ from those representing the CW model, which includes a detailed three-dimensional representation of the honeycomb geometry. The first step involves isolating the nodes and associated displacement vectors corresponding exclusively to the top and bottom skins. Then, it is necessary to normalize the extracted modal vectors, to remove any scaling factors arising from differences in the modelling approaches. This ensures that the subsequent comparisons reflect the intrinsic geometric characteristics of the mode shapes rather than arbitrary amplitude differences. The normalization yields unit-norm vectors for both CW and LW sets. Finally, by superimposing the three-dimensional nodal displacement field to the undeformed base grid, it is possible to plot the skins modal shapes for the two theories, as reported in Fig. 14 for some illustrative modes, and in Fig. 15 highlighting in detail the differences for a selected mode with significant local effects.

Following normalization, it is necessary to address the spatial discrepancy between the two sets of data. As evident from the comparisons of Fig. 14, the nodal distributions in the LW and CW models are not coincident; therefore, a direct comparison of the displacement fields is not possible. To overcome this, both sets of modal data are interpolated onto a common spatial grid. The choice of the common grid is essential, as it should cover the entire domain of the skins and be sufficiently refined to capture the essential features of the mode shapes. The common grid is defined over the region of interest, and a linear interpolation is applied to the skins modal shapes. This technique maps the displacement values from the original non-coincident nodal positions of LW and CW models onto the common grid. The result is two sets of displacement fields, one for the LW model and one for the CW model, defined at identical spatial coordinates. The interpolation process is verified to preserve the morphological features of the original mode shapes; the skins interpolated mode shapes are reported in Fig. 16 for the two sets of illustrative modes, LW and CW, respectively, and in Fig. 17 to show in detail the differences for a mode with important local effects.

Once both the LW and CW displacement fields are mapped onto the common grid, MAC can be computed. MAC value ranges from 0 to 1, with 0 indicating no correlation and 1 indicating perfect correlation between the mode shapes. High MAC values indicate that the LW and CW models produce similar deformation patterns for the skins, despite the inherent differences in the underlying modelling assumptions. Conversely, low MAC values suggest significant discrepancies between the two sets of modal shapes. The results of the MAC analysis offer a quantitative basis for assessing the degree of correlation between the modal shapes produced by the two modelling approaches. The implementation of the MAC involves a pointwise comparison across the common grid. This analysis is particularly useful when the modal correspondence between the models is not one-to-one, as discussed in previous section. In such cases, the MAC serves as an objective tool for pairing modes that exhibit the highest degree of similarity, thus enabling a more rigorous comparison of the natural frequencies associated with these modes. For the LW and CW skins mode shapes comparison, the MAC diagram is reported in Fig. 18.

The outcomes of the MAC diagram analysis support the discussion made in the Section 3.1. Indeed, analysing the MAC diagram, it is

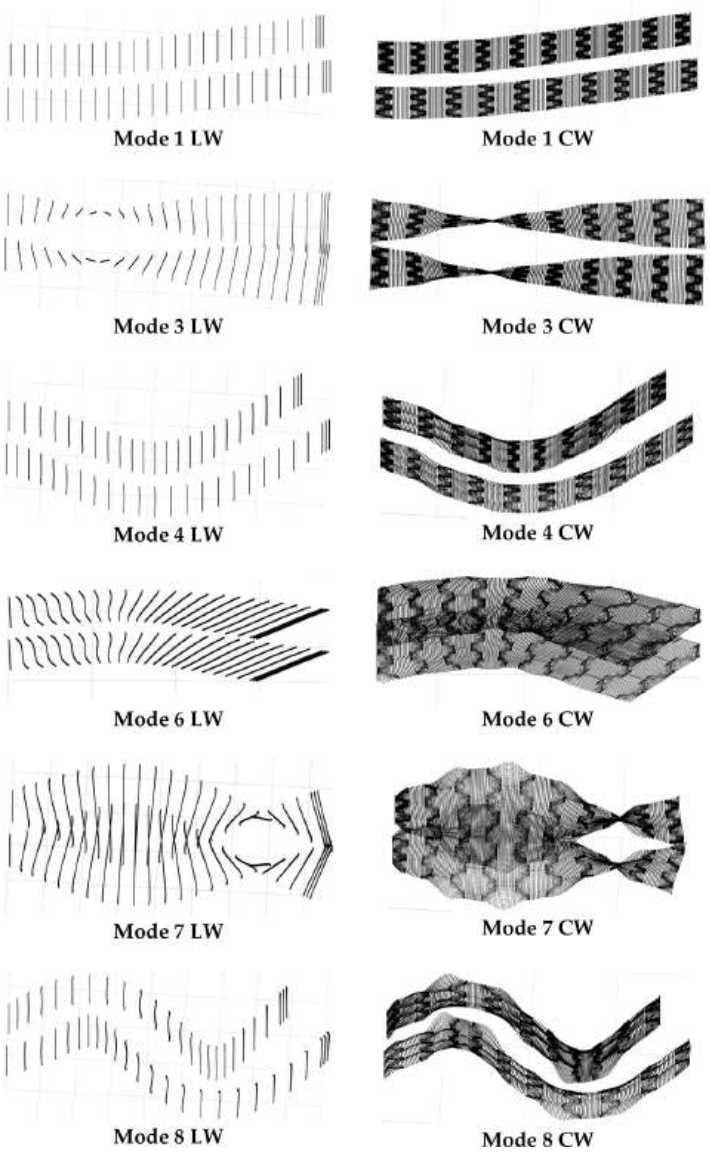


Fig. 14. Mode shapes of skins for the LW (left) and CW (right) models.

evident that the first modes exhibit high similarity, approaching unity, indicating a strong correspondence between the LW and CW modal shapes for the skins. As the mode order increases, the MAC coefficients decrease, revealing a lower similarity between the two models. This observation suggests that CW captures more localized dynamic features, which the LW approach partially simplifies. Moreover, the presence of some significant off-diagonal values indicates potential mode mixing. Nonetheless, the main diagonal maintains a good agreement between LW and CW for low- and mid-frequency modes, confirming that, on a global scale, the skins are modelled in a relatively consistent manner by both theories. For higher-frequency modes, the MAC diagram shows a progressive decline in correlation coefficients, highlighting an increasing divergence between the two predictions. This phenomenon typically arises when local modelling details, such as those included in CW, are crucial for describing more complex dynamics, which LW does not capture as accurately. As a result, CW demonstrates superior performance in high-frequency mode simulations by incorporating more localized effects. This finding confirms the superiority of the CW model for more detailed analyses, even though at a higher modelling complexity and computational cost than the LW theory.

The procedure described here is robust and adaptable. It can be applied to other scenarios where model comparisons are required, especially in cases where the theoretical model and the geometrical discretization differ significantly. The isolation of specific portion of interest of the model, together with the use of a common interpolation grid, is a key step that ensures the comparability of data sets derived from different numerical methods.

4. Discussion

A first key point emerged from the application of the approach provided in this paper involves the general practical rationale of CUF CW strategy for thin-walled dynamics analysis. The results discussed in Section 3.1 show that the CUF CW formulation provides a unique and powerful high-fidelity tool to resolve local, high-frequency phenomena in honeycomb-cored plates. Beyond the numerical figures, it is important to articulate why CW constitutes a practically superior method for complex thin-walled structures, i.e. configurations where thickness is orders of magnitude smaller than in-plane dimensions and where interfaces between dissimilar parts are prevalent. To illustrate this point clearly, it is necessary to give particular attention to the limitations of solid-element 3D FEM for thin parts. When thin walls are modelled with

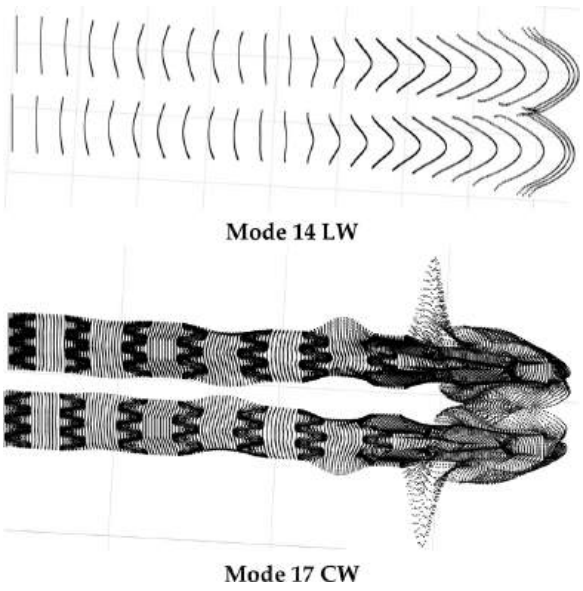


Fig. 15. Detail of skins' mode shape comparison for a mode with significant local effects.

solid elements, accurate thickness representation typically requires at least two or three elements across the thickness to properly control through-thickness gradients. This immediately induces unfavourable aspect ratios, e.g. elements crushed through thickness, mesh distortion, and a general deterioration of element performance. To mitigate this, the mesh must be drastically refined through the thickness, which causes a rapid growth of the total DoFs and a substantial increase in memory required and computational time. The situation becomes even more challenging in the presence of geometric transitions, as thin skins bonded to thicker subcomponents, stiffeners, junctions: generating a conformal 3D mesh that remains well-conditioned across disparate length scales is very difficult and may introduce numerical instability.

For sandwich panels, a purely 3D FE approach requires an explicit discretization of every structural component. In honeycomb cores, the cell walls could be extremely thin relative to their in-plane size; resolving such details in 3D requires a drastic refinement in the wall direction and around ligaments, rapidly pushing the model beyond practical limits; it also increases material interfaces that must be consistently defined, meshed, and tied, each representing a potential source of modelling error and cost. Similar issues arise for metamaterial-inspired cores with fine features and multiple phases.

The CW strategy replaces the need for a conformal 3D solid mesh with a section-based description and a 1D axial discretization. In practical terms, the modelling consists of two steps: build a cross-section mesh that explicitly resolves also thin walls and local details and define the beam axis and its discretization, which governs the longitudinal variation while keeping the number of degrees of freedom moderate. Kinematic continuity at interfaces between dissimilar parts is imposed at the section level, so no conformal 3D grid or ad-hoc multi-point constraints are required across sharp thickness transitions. In practice, this section-centric resolution provides the local geometric fidelity needed to capture local mechanics, high-frequency phenomena where they originate (e.g. at interfaces), while the axial line mesh prevents the DoF huge increase typical of solid 3D models attempting to pack 2 or more elements across very small thicknesses. The result is a robust and scalable modelling route for thin and very thin assemblies, avoiding the core bottlenecks of 3D solids without procedural or modelling overhead. Although honeycomb plates are adopted here because they constitute a stringent benchmark for geometrical complexity and local dynamic effects, the method itself is component-agnostic. In the same CUF CW setting, it is possible to model stiffeners, stringers, spars, bonded joints, inserts, and alternative cores (e.g., foam or metamaterial lattices) by changing only the cross-sectional discretization, see refs., [45,46]; the coupling across parts still follows the same CUF kinematic continuity. No procedural changes are required in the assembly or solution. In other words, the generality of CW directly derives from its section-based nature, regardless of the geometric complexity. The evidence presented in Section 3.1 indicates that, while ESL and LW remain attractive for global predictions at very low cost, they inherently miss local, high-order phenomena; CW, instead, resolves those effects with a modelling effort that is not procedurally more complex than ESL/LW and with the need of a moderate computational effort, in terms of degrees of freedom.

5. Conclusions

This study has provided a comparative analysis of the modal response of sandwich structures with honeycomb cores, employing three distinct modelling approaches within the Carrera Unified Formulation framework: Equivalent Single Layer, Layer-Wise, and Component-Wise theories. The investigation supported the discussion of the advantages and limitations of each approach in capturing both global and local vibrational characteristics of the structure. The results demonstrate that ESL and LW models, while computationally efficient, easy to model and potentially effective if global deformations are considered, introduce significant simplifications through core homogenization, leading to discrepancies in the estimation of natural frequencies and mode shapes, particularly for high-frequency modes characterized by local deformations. This aspect has direct engineering relevance, since short-wavelength responses are central to vibro-acoustic transmission, impact-related events, and aeroelastic phenomena in lightweight aerospace components. Specifically, the ESL formulation tends to overestimate torsional stiffness and underestimate extensional behaviour, whereas the LW theory offers a more refined representation but still lacks the ability to resolve detailed local effects. For LW, the observed discrepancies result in a general underestimation of natural frequencies, with deviations reaching up to approximately −19 % within the first ten modes. In contrast, the CW approach, which explicitly models the core and skins as independent subdomains, proves to be the most accurate in capturing both global and local dynamic behaviours. The CW model aligns closely with high-fidelity finite element simulations while requiring substantially fewer degrees of freedom, highlighting the efficiency of CUF-based simulative approach, and clarifying the practical cost–accuracy trade-off that guides model selection. The results also emphasize that CW modelling is indispensable when detailed local effects and complex interactions between the core and skins play a critical role in structural performance; this is typical for advanced multi-layered structures, as sandwich with honeycomb core. Importantly, these conclusions are not restricted to the specific case analysed: Appendix A shows that they persist under a markedly different honeycomb arrangement, whereas Appendix B offers the application of the same framework to a case with different boundary conditions, supporting the case-independent nature of the proposed methodology. The insights proposed by this study contribute to a more informed selection of modelling approaches for dynamic analysis of honeycomb sandwich structures, highlighting the potential of CUF as an efficient tool for advanced structural analysis. Accordingly, the present contribution is methodological rather than design-oriented: comprehensive parametric studies on the influence of cell geometry and skin/core properties on dynamic properties are envisaged as future work. These should also explore the extension of the present methodology to nonlinear dynamic analyses, investigating the role of geometric and material non-linearities in sandwich structures. Furthermore, the extension of the approach to more complex geometries and metamaterial-like structures could open the study of efficient structures for tailored advanced applications. A concluding note about some model limitations: the analyses reported here assume perfect bonding between skins and core. Phenomena such

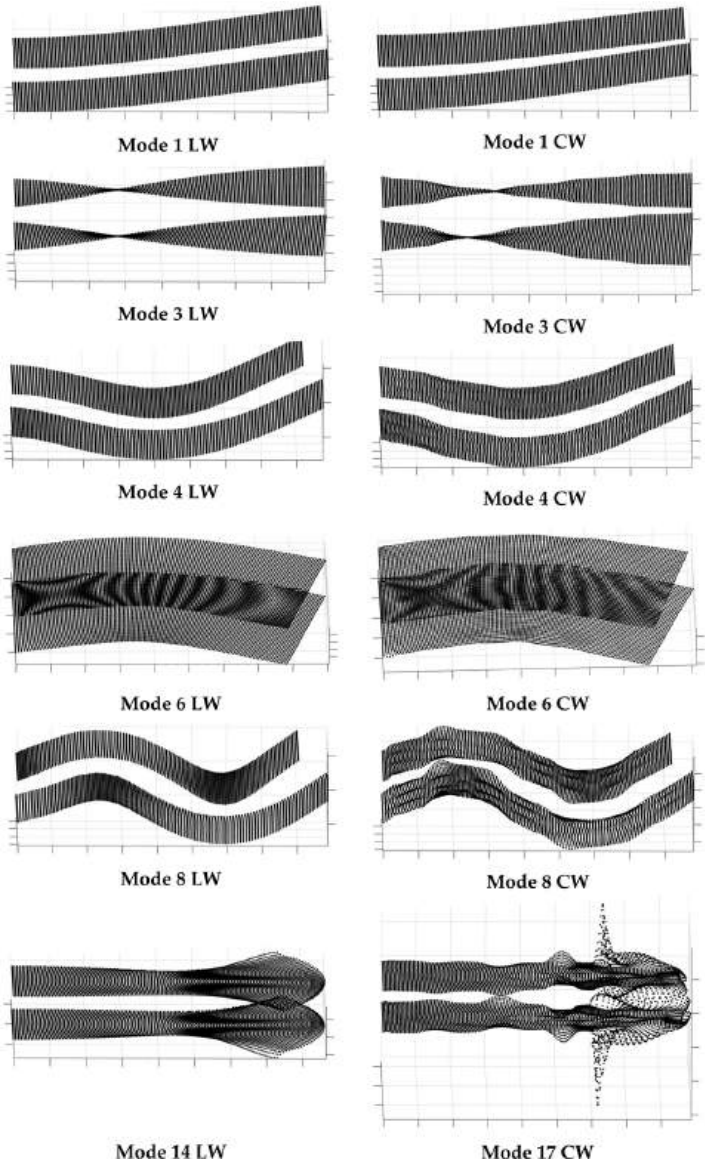


Fig. 16. Interpolated skins' mode shapes for LW (left) and CW (right) models.

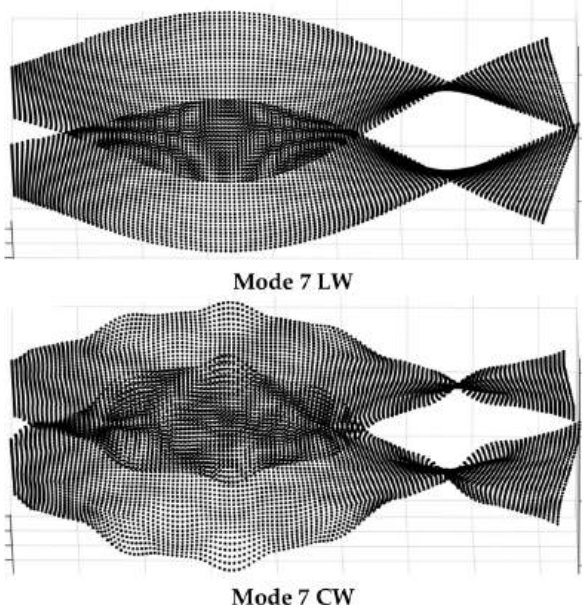


Fig. 17. Detail of interpolated skins' mode shape for a mode with relevant local effects.

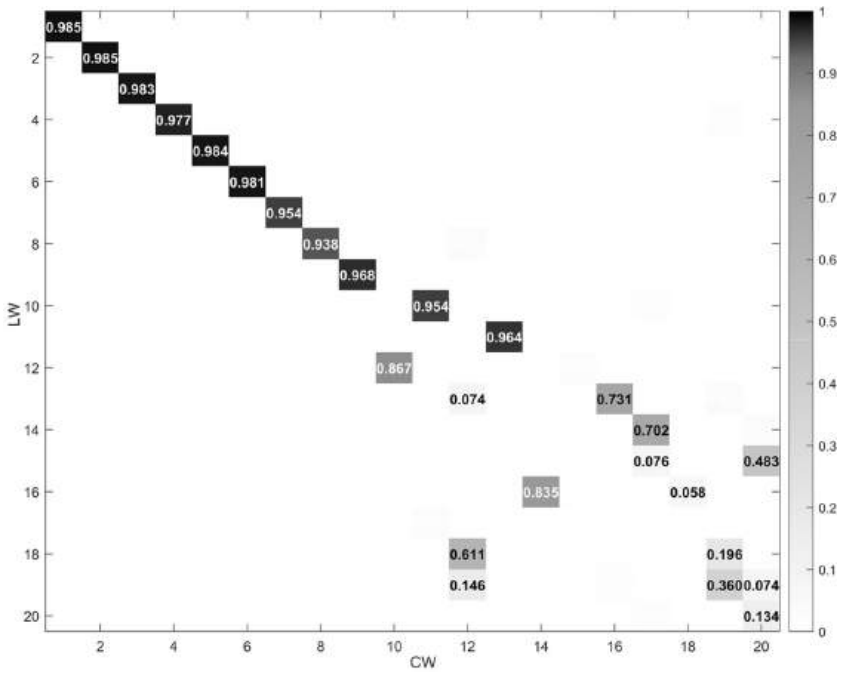


Fig. 18. MAC diagram for LW and CW skins mode shapes.

as imperfections or interfacial debonding are not addressed, as their treatment would require additional constitutive assumptions and would effectively pose a different mechanical problem. These application-specific extensions are important yet beyond the present scope; such an extension involves dedicated validation campaign and it will be addressed in future work.

CRediT authorship contribution statement

E. Carrera: Writing – review & editing, Supervision, Resources, Project administration, Methodology, Investigation, Data curation, Conceptualization. **K. Abu Salem:** Writing – original draft, Visualization, Methodology, Investigation, Formal analysis, Data curation, Conceptualization. **R. Augello:** Writing – review & editing, Validation, Methodology, Investigation, Data curation, Conceptualization.

Declaration of competing interest

The authors declare that they have no known competing financial interests or personal relationships that could have appeared to influence the work reported in this paper.

Appendix A

This appendix presents the results of the modal analysis conducted on a different sandwich panel, characterized by a geometry distinct from that of the panel examined in the main body of the paper. Specifically, this aluminium panel features a larger core cross-sectional area, a reduced overall height, a smaller hexagonal unit, and a core composed of a significantly higher number of densely packed cells. Dimensions and details are summarized in Figs. A.1 and A.2.

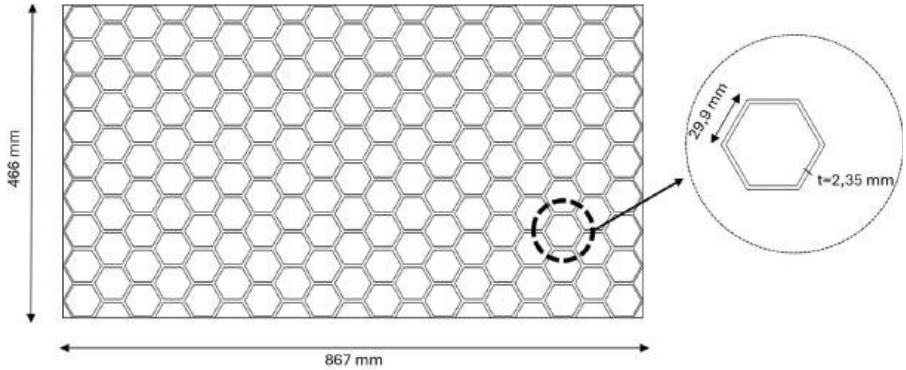


Fig. A.1. Core geometry.



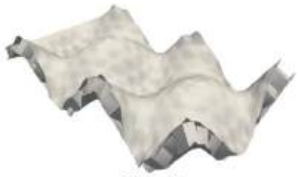
Fig. A.2. View of the sandwich panel.

Tables A.1 and A.2 report mode shapes and frequencies computed for this sandwich panel with both LW and CW approaches. Specifically, some modes involving global deformations are reported in Table A.1, whereas some modes with more evident local effects are reported in Table A.2. In general, the same considerations presented in the main body of the paper also apply to this geometry, demonstrating the general applicability of the approach. Local effects, most notably skin deformation, become apparent at Mode 22 (Table A.2). Once these phenomena arise, the frequency discrepancy between the homogenized LW model and the refined CW model grows markedly. The same pattern is evident in the main study, where local behaviour starts to appear at Modes 6 and 7. This result demonstrates that, for higher modes, local phenomena occur for structure with more cells, so a CW model is mandatory to accurately predict the associated frequency.

Table A.1
Mode shapes and frequencies – pt.1.

LW	CW
 Mode 1 f = 0.041 kHz	 Mode 1 f=0.044 kHz
 Mode 2 f=0.142 kHz	 Mode 2 f=0.163 kHz
 Mode 4 f=0.244 kHz	 Mode 4 f=0.269 kHz
 Mode 5 f=0.463 kHz	 Mode 5 f=0.523 kHz
 Mode 6 f=0.658 kHz	 Mode 6 f=0.726 kHz
 Mode 10 f=0.918 kHz	 Mode 9 f=1.001 kHz

Table A.2
Mode shapes and frequencies – pt.2.

LW	CW
 Mode 22 f = 2.409 kHz	 Mode 22 f=2.689 kHz
 Mode 27 f=2.835 kHz	 Mode 24 f=3.055 kHz
 Mode 25 f=2.769 kHz	 Mode 25 f=3.102 kHz
 Mode 29 f=2.874 kHz	 Mode 26 f=3.180 kHz
 Mode 30 f=2.992 kHz	 Mode 27 f=3.265 kHz

Appendix B

This appendix reports results for a case with boundary conditions different from those discussed in the main text: the sandwich panel is clamped at both end sections (clamped–clamped). The purpose is to support the generality of the proposed CUF-based approach, which does not depend on nor is limited by the choice of boundary conditions. Table B.1 presents, for the clamped-clamped case, the natural frequencies and the comparison of the ESL, LW, and CW formulations, following the same rationale discussed in the main body of the paper.

Table B.1
First eight natural frequencies for the clamped-clamped configuration.

	CUF ESL		CUF LW		CUF CW	
	f [kHz]	Δ%	f [kHz]	Δ%	f [kHz]	Δ%
Mode 1	3.268	-12.5	3.353	-0.5	3.37	ref.
Mode 2	3.586	-16.1	3.764	-12.2	4.286	
Mode 3	7.155	28.8	4.888	-0.4	4.904	
Mode 4	8.122	-6.4	7.435	-3.1	7.669	

(*continued on next page*)

Table B.1 (*continued*)

	CUF ESL		CUF LW		CUF CW	
	f [kHz]	Δ%	f [kHz]	Δ%	f [kHz]	Δ%
Mode 5	7.149	-13.9	7.388	-14.6	8.644	
Mode 6	8.049	-5.6	8.369	-3.8	8.701	
Mode 7	7.725	15.7	10.221	3.3	9.892	
Mode 8	11.399	-2.2	11.599	-7.7	12.567	

Data availability

Data will be made available on request.

References

[1] N.K. Chandrasekaran, V. Arunachalam, State-of-the-art review on honeycomb sandwich composite structures with an emphasis on filler materials, Polym. Compos. 42 (2021) 5011–5020, https://doi.org/10.1002/pc.26252.

[2] J.K. Paik, A.K. Thayamballi, G.S. Kim, The strength characteristics of aluminum honeycomb sandwich panels, Thin-walled Struct. 35 (1999) 205–231, https://doi.org/10.1016/S0263-8231(99)00026-9.

[3] M.S. Al-Khazraji, S.H. Bakhy, J.M. Jweeg, M. J, Composite sandwich structures: review of manufacturing techniques, J. Eng. Des. Technol. 22 (5) (2024) 1616–1636, https://doi.org/10.1108/JEDT-03-2022-0141.

[4] Z. Sun, S. Shi, X. Guo, X. Hu, H. Chen, On compressive properties of composite sandwich structures with grid reinforced honeycomb core, Compos. B: Eng. 94 (2016) 245–252, https://doi.org/10.1016/j.compositesb.2016.03.054.

[5] X. Zhao, L. Wei, D. Wen, G. Zhu, Q. Yu, Z.D. Ma, Bending response and energy absorption of sandwich beams with novel auxetic honeycomb core, Eng. Struct. 247 (2021) 113204, https://doi.org/10.1016/j.engstruct.2021.113204.

[6] X.L. Gai, X.W. Guan, Z.N. Cai, X.H. Li, W.C. Hu, T. Xing, F. Wang, Acoustic properties of honeycomb like sandwich acoustic metamaterials, Appl. Acoust. 199 (2022) 109016, https://doi.org/10.1016/j.apacoust.2022.109016.

[7] V. Tahmasbi, S. Noori, Thermal analysis of honeycomb sandwich panels as substrate of ablative heat shield, J. Thermophys. Heat Transf. 32 (2018) 129–140, https://doi.org/10.2514/1.T5051.

[8] M. Ruzzene, Vibration and sound radiation of sandwich beams with honeycomb truss core, J. Sound. Vib. 277 (2004) 741–763, https://doi.org/10.1016/j.jsv.2003.09.026.

[9] L. Wang, Z. Yang, T.P. Waters, Structural damage detection using cross correlation functions of vibration response, J. Sound. Vib. 329 (2010) 5070–5086, https://doi.org/10.1016/j.jsv.2010.06.020.

[10] N. Namazinia, A. Alibeigloo, M. Karimiasl, Free vibration and static analysis of sandwich composite plate with auxetic core and GPLRC facing sheets in hygrothermal environment, Forces Mech. 15 (2004) 100264, https://doi.org/10.1016/j.finmec.2024.100264.

[11] Y. Wang, Z. Zhang, X. Xue, L. Zhang, Free vibration analysis of composite sandwich panels with hierarchical honeycomb sandwich core, Thin-Walled Struct. 145 (2019) 106425, https://doi.org/10.1016/j.tws.2019.106425.

[12] N. Namazinia, A. Alibeigloo, M. Karimiasl, Vibration analysis of a composite sandwich plate with a viscoelastic auxetic core, FG-CNTRC interior, and MEE–FGP exterior face sheets, Mech. Based Des. Struct. Mach. 53 (2) (2025) 1447–1493, https://doi.org/10.1080/15397734.2024.2386134.

[13] M.S. Al-Khazraji, M.J. Jweeg, S.H. Bakhy, Free vibration analysis of a laminated honeycomb sandwich panel: a suggested analytical solution and a numerical validation, J. Eng. Des. Technol. 22 (2) (2024) 316–343, https://doi.org/10.1108/JEDT-10-2021-0536.

[14] C. Hong, S.J. Elliott, Local coupling between actuator and sensor pairs in light honeycomb structures, J. Sound. Vib. 302 (2007) 117–137, https://doi.org/10.1016/j.jsv.2006.11.006.

[15] N. Namazinia, A. Alibeigloo, M. Karimiasl, Vibration characteristics of a sandwich plate with viscoelastic auxetic core and graphene nanoplatelets reinforced skins, Arch. Civ. Mech. Eng. 25 (1) (2024) 49, https://doi.org/10.1007/s43452-024-01072-8.

[16] Z. Zhou, M. Chen, Y. Li, Application scope studies of analytical methods based on the equivalent single-layer and layerwise theories for vibration analysis of symmetric sandwich plates, Acta Mech. 234 (2023) 377–401, https://doi.org/10.1007/s00707-022-03392-3.

[17] R.A. Moreira, J.D. Rodrigues, A layerwise model for thin soft core sandwich plates, Comput. Struct. 84 (2006) 1256–1263, https://doi.org/10.1016/j.compstruc.2006.01.020.

[18] I. Kreja, A. Sabik, Equivalent single-layer models in deformation analysis of laminated multilayered plates, Acta Mech. 230 (2019) 2827–2851, https://doi.org/10.1007/s00707-019-02434-7.

[19] S. Abrate, M. Di Sciuva, Equivalent single layer theories for composite and sandwich structures: a review, Compos. Struct. 179 (2017) 482–494, https://doi.org/10.1016/j.compstruct.2017.07.090.

[20] D. Li, Layerwise theories of laminated composite structures and their applications: a review, Arch. Comput. Methods Eng. 28 (2021) 577–600, https://doi.org/10.1007/s11831-019-09392-2.

[21] M. Amabili, J.N. Reddy, Nonlinear mechanics of sandwich plates: layerwise third-order thickness and shear deformation theory, Compos. Struct. 278 (2021) 114693, https://doi.org/10.1016/j.compstruct.2021.114693.

[22] M. Amabili, J.N. Reddy, The nonlinear, third-order thickness and shear deformation theory for statics and dynamics of laminated composite shells, Compos. Struct. 244 (2020) 112265, https://doi.org/10.1016/j.compstruct.2020.112265.

[23] B. Wang, Y. Wei, S. Yuan, W. Hao, C. Tang, Enhanced bending performance of assembly honeycomb structure sandwich panels: effects of core configuration and local reinforcement, Thin-Walled Struct. (2025) 113597, https://doi.org/10.1016/j.tws.2025.113597.

[24] S. Xu, H. Huang, Q. Fu, X. Guang, X. Deng, Design, study and optimization of crashworthiness and energy absorption of symmetric and asymmetric offset hexagonal honeycombs, Thin-Walled Struct. (2025) 113556, https://doi.org/10.1016/j.tws.2025.113556.

[25] M. Amabili, Shell–plate interaction in the free vibrations of circular cylindrical tanks partially filled with a liquid: the artificial spring method, J. Sound. Vib. 199 (1997) 431–452, https://doi.org/10.1006/jsvi.1996.0650.

[26] E. Carrera, M. Cinefra, M. Petrolo, E. Zappino, Finite Element Analysis of Structures Through Unified Formulation, John Wiley & Sons, West Sussex, United Kingdom, 2014.

[27] J. Gibson, M. Ashby, Cellular Solids: Structure and Properties, Cambridge University Press, 1997, https://doi.org/10.1017/CBO9781139878326.

[28] N. Ahmed, N. Zafar, H.Z. Janjua, Homogenization of honeycomb core in sandwich structures: a review, in: 16th International Bhurban Conference on Applied Sciences and Technology (IBCAST IEEE), Islamabad, Pakistan, 2019, pp. 159–173, https://doi.org/10.1109/IBCAST.2019.8667144.

[29] C.W. Schwingshackl, G. Aglietti, P.R. Cunningham, Determination of honeycomb material properties: existing theories and an alternative dynamic approach, J. Aerosp. Eng. 19 (2006) 177–183, https://doi.org/10.1061/(ASCE)0893-1321(2006)19:3(177).

[30] W.S. Burton, A.K. Noor, Assessment of continuum models for sandwich panel honeycomb cores, Comput. Methods Appl. Mech. Eng. 145 (1997) 341–360, https://doi.org/10.1016/S0045-7825(96)01196-6.

[31] E. Sather, T. Krishnamurthy, An analytical method to calculate effective elastic properties of general multifunctional honeycomb cores in sandwich composites, NASA Technical Memorandum, NASA/TM-2019-220275, https://ntrs.nasa.gov/citations/20190025271, 2019.

[32] M. Yasin, K.F. Brethee, H.M. Hassan, A study of honeycomb sandwich structure dynamically equivalent modeling methods based on phenotypic analysis and comparison, AIP. Conf. Proc. 3009 (2024), https://doi.org/10.1063/5.0190813.

[33] M. Moeini, M. Begon, M. Lévesque, Numerical homogenization of a linearly elastic honeycomb lattice structure and comparison with analytical and experimental results, Mech. Mater. 167 (2022) 104210, https://doi.org/10.1016/j.mechmat.2022.104210.

[34] S. Sorohan, M. Sandu, A. Sandu, D.M. Constantinescu, Finite element models used to determine the equivalent in-plane properties of honeycombs, Mater. Today: Proc. 3 (2016) 1161–1166, https://doi.org/10.1016/j.matpr.2016.03.013.

[35] G. Caprino, A. Langella, Study of a three-point bending specimen for shear characterisation of sandwich cores, J. Compos. Mater. 34 (2000) 791–814, https://doi.org/10.1177/002199830003400904.

[36] F. Mujika, J. Pujana, M. Olave, On the determination of out-of-plane elastic properties of honeycomb sandwich panels, Polym. Test. 30 (2011) 222–228, https://doi.org/10.1016/j.polymertesting.2010.12.005.

[37] A. Kumar, N. Muthu, R.G. Narayanan, Equivalent orthotropic properties of periodic honeycomb structure: strain-energy approach and homogenization, Int. J. Mech. Mater. Des. 19 (2023) 137–163, https://doi.org/10.1007/s10999-022-09620-x.

[38] E. Carrera, Theories and finite elements for multilayered plates and shells: a unified compact formulation with numerical assessment and benchmarking, Arch. Comput. Methods Eng. 10 (2003) 215–296, https://doi.org/10.1007/BF02736224.

[39] H. Meyer-Piening, Experiences with 'exact' linear sandwich beam and plate analyses regarding bending, instability and frequency investigations, in: Proceedings of the Fifth International Conference On Sandwich Constructions, Zurich, Switzerland, 2000, pp. 37–48. September 5–7.

[40] E. Carrera, A. Ciuffreda, Bending of composites and sandwich plates subjected to localized lateral loadings: a comparison of various theories, Compos. Struct. 68 (2005) 185–202, https://doi.org/10.1016/j.compstruct.2004.03.013.

[41] K. Abu Salem, R. Augello, E. Carrera, Component-wise modelling of core and skin in sandwich structures using a single refined beam finite element, Mech. Adv. Mater. Struct. (2025) 1–14, https://doi.org/10.1080/15376494.2025.2458237.
[42] V. Pourriahi, M. Heidari-Rarani, A.T Isfahani, Influence of geometric parameters on free vibration behavior of an aluminum honeycomb core sandwich beam using experimentally validated finite element models, J. Sandw. Struct. Mater. 24 (2) (2022), https://doi.org/10.1177/10996362211053633.
[43] M. Pastor, M. Binda, T. Harčarik, Modal assurance criterion, Procedia Eng. 48 (2012) 543–548, https://doi.org/10.1016/j.proeng.2012.09.551.
[44] M. Amabili, G. Dalpiaz, Breathing vibrations of a horizontal circular cylindrical tank shell, partially filled with liquid, J. Vib. Acoust. 117 (1995) 187–191, https://doi.org/10.1115/1.2873885.
[45] E. Carrera, A. Pagani, A. M. Petrolo, Free vibrations of damaged aircraft structures by component-wise analysis, AIAA J. 54 (10) (2016) 3091–3106, https://doi.org/10.2514/1.J054640.
[46] R. Augello, E. Carrera, W.Q. Chen, B. Wu, Y.Z. Wang, Nonlinear static analysis of metamaterial structures based on the Kagome lattice using beam finite elements and component-wise approach, Int. J. Solids. Struct. 318 (2025) 113387, https://doi.org/10.1016/j.ijsolstr.2025.113387.